Fully numerical Hartree–Fock and density functional calculations. II. Diatomic molecules

Susi Lehtola

March 11, 2019

Department of Chemistry, University of Helsinki, P.O. Box 55 (A. I. Virtasen aukio 1), FI-00014 University of Helsinki, Finland

susi.lehtola@alumni.helsinki.fi

Abstract

We present the implementation of a variational finite element solver in the HelFEM program for benchmark calculations on diatomic systems. A basis set of the form $\chi_{nlm}(\mu,\nu,\phi) = B_n(\mu)Y_l^m(\nu,\phi)$ is used, where (μ,ν,ϕ) are transformed prolate spheroidal coordinates, $B_n(\mu)$ are finite element shape functions, and Y_l^m are spherical harmonics. The basis set allows for an arbitrary level of accuracy in calculations on diatomic molecules, which can be performed at present with either nonrelativistic Hartree–Fock (HF) or density functional (DF) theory. Hundreds of DFs at the local spin-density approximation (LDA), generalized gradient approximation (GGA) and the meta-GGA level can be used through an interface with the Libxc library; meta-GGA and hybrid DFs aren't available in other fully numerical diatomic program packages. Finite electric fields are also supported in HelFEM, enabling access to electric properties.

We introduce a powerful tool for adaptively choosing the basis set by using the core Hamiltonian as a proxy for its completeness. HelFEM and the novel basis set procedure are demonstrated by reproducing the restricted open-shell HF limit energies of 68 diatomic molecules from the 1$^{\text{st}}$ to the 4$^{\text{th}}$ period with excellent agreement with literature values, despite requiring *orders of magnitude* fewer parameters for the wave function. Then, the electric properties of the BH and N_2 molecules under finite field are studied, again yielding excellent agreement with previous HF limit values for energies, dipole moments, and dipole polarizabilities, again with much more compact wave functions than what were needed in the literature references. Finally, HF, LDA, GGA, and meta-GGA calculations of the atomization energy of N_2 are performed, demonstrating the superb accuracy of the present approach.

1 Introduction

In the first part of this series,[1] we presented fully numerical Hartree–Fock (HF) and density functional calculations on atoms. The present manuscript focuses on diatomic molecules, which may serve as even more stringent tests of *ab initio* as well as density functional methods than atoms, as the methods' accuracy can be probed for multiple kinds of covalent bonds, as well as for ionic bonds and dispersion effects. As reviewed at length in ref. 2, the history of fully numerical calculations on diatomic molecules is almost as long as that on atoms, starting with the partial wave approach of McCullough.[3,4] The partial wave approach appears to have since fallen out of use, with the well-known programs by Heinemann, Laaksonen, Sundholm, Kobus and coworkers[5–8] relying on grid-based approaches for the angular expansion.

However, it is not clear whether the partial wave approach should be fully forgotten: on the contrary, there is a strong argument for resuscitating its use. Unlike in the fully grid-based approaches (see references in ref. 2), in the partial wave approach angular integrals can be evaluated analytically in closed form, requiring no approximations or truncations to be made in the numerical implementation beyond the choice of the single-particle basis set. This is especially true for the two-electron integrals: as with the Legendre expansion

in the atomic case,[1] the angular integrals arising for diatomic molecules from the Neumann expansion[9] can be performed analytically within the partial wave expansion,[4] indicating that such a basis is extremely convenient for calculations.

While a suitable variational re-implementation of McCullough's partial-wave approach has been reported in ref. 10 employing a basis spline approach, the calculations therein were limited to first and second period atoms and diatomic molecules, leaving it unclear whether the approach is tractable for heavier systems. As we were furthermore unable to obtain a copy of the program of ref. 10, we decided to write a new finite element program from scratch, employing modern programming paradigms and libraries. Some omissions in the equations of ref. 10 were thereby found, as shall be described below. We have also developed faster algorithms for the formation of the Coulomb and exchange matrices, which do not appear to have been used in ref. 10. Finally, unlike the program of ref. 10, the present implementation is parallellized, and also supports calculations within density functional theory[11,12] (DFT) in addition to the HF calculations of ref. 10.

In the present work, we will thus describe the implementation of a finite element solver for HF and DFT on diatomic molecules, employing the partial wave approach originally proposed by McCullough.[3,4] The program is called HelFEM[13] for the city and university of Helsinki where the present author is situated, and for the electronic Hamiltonian

$$\hat{H}_{el} = -\frac{1}{2}\sum_i \nabla_i^2 - \sum_i \frac{Z_A}{r_{iA}} - \sum_i \frac{Z_B}{r_{iB}} + \sum_{i>j} \frac{1}{r_{ij}} + \frac{Z_A Z_B}{r_{AB}}, \tag{1}$$

and for the finite element method (FEM). HelFEM is open source (GNU General Public License) and it has been written in object-oriented C++. Several recently published open source algorithms and libraries are used in HelFEM. HelFEM is especially linked to the Libxc library,[14] which provides hundreds of local spin density approximation[12] (LDA), generalized-gradient approximation[15] (GGA) as well as meta-GGA[16] exchange-correlation functionals. In contrast, the programs by Heinemann, Laaksonen, Sundholm, Kobus and coworkers[5–8] are limited to few LDA and GGA functionals; to our knowledge, meta-GGAs have not been previously available in all-electron diatomic programs.

Both pure and global hybrid density functionals are supported in HelFEM; alike the atomic calculations discussed in ref. 1, range-separated functionals are not yet supported for obvious reasons that are discussed below. Both spin-restricted, spin-restricted open-shell, as well as spin-unrestricted calculations are supported in HelFEM. As far as we know, spin-unrestricted all-electron real-space calculations on diatomics have only been reported so far by Heinemann and coworkers.[17,18]

As was discussed in part I for the atomic calculations,[1] the data layout in HelFEM is deliberately similar to what is used in typical Gaussian-basis quantum chemistry programs; this also holds in the case of diatomic calculations. Thanks to this, many functionalities, such as the DIIS[19,20] and ADIIS[21] self-consistent field (SCF) procedure convergence accelerators have been adopted directly from the Erkale program.[22,23] In addition, interfaces to multiconfigurational methods,[24] configuration interaction, and coupled-cluster theories[25] available in *e.g.* Psi4[26] or PySCF[27] could be implemented in the future.

Unlike the commonly used programs for fully numerical calculations on diatomic molecules by Heinemann, Laaksonen, Sundholm, Kobus and coworkers,[5–8] HelFEM calculates the Coulomb and exchange matrices in the "traditional" manner with two-electron integrals. This means that the value for the practical infinity r_∞ can be determined by the behavior of the electron density alone. Furthermore, the approach in HelFEM is strictly variational: the energies given by the program are true upper bounds to the energy computed in a complete basis set (CBS). This can be contrasted to the energies produced *e.g.* by the x2dhf program,[7,8] which are typically antivariational, *i.e.* the energy approaches the converged value from below due to inaccuracies in the potential. Because, for instance, the HF energy is an upper bound to the energy of the *many-electron* wave function, it is clearly beneficial if the HF energy itself is also estimated variationally by the numerical approach. Although both numerical approaches give the same solution at convergence,[28] variationality makes it easier to establish convergence to the basis set limit.

Furthermore, the approach in HelFEM guarantees smooth and rapid convergence of the SCF procedure without the need to adjust relaxation parameters as in x2dhf. An initial guess wave function or orbital symmetries are also unnecessary in HelFEM, unlike for x2dhf or the program by Heinemann and coworkers; this again greatly simplifies running calculations. Finally, unlike the finite difference approach used in x2dhf where smaller grid spacings radically increase the number of steps to solution, the speed of SCF convergence

in HelFEM is not affected by the size of the basis set. Although the diagonalization cost is affected by the use of a larger basis set, it is not rate determining in our calculations.

The layout of the article is the following. Next, in the Theory section, we will present all the equations that are necessary for a finite element implementation of the partial-wave approach for diatomic molecules, as well as present a novel adaptive approach for choosing the basis set cost-efficiently for diatomic calculations. The Theory section is followed by a Computational Details section, which describes the present implementation and details various convergence parameters that were used for the calculations. The Results section shows three applications of the novel program: the calculation of restricted open-shell HF (ROHF) limit ground state energies of 70 diatomic molecules from refs. 29 and 30 that range from the 1^{st} to the 4^{th} period, the finite field electric properties of the BH and N_2 molecules at the HF limit, and the atomization energy of N_2 with HF, as well as LDA, GGA, and meta-GGA functionals. The article ends with brief Summary and Conclusions sections.

As the article relies on knowledge on the finite element approach that was presented in the first part of this series,[1] it should be read first. Atomic units are used unless specified otherwise. The Einstein summation convention is used, meaning summations are implied over repeated indices.

2 Theory

2.1 Coordinate system

Modified prolate spheroidal coordinates (μ, ν, ϕ) due to Becke[31] (see illustrations in ref. 2) are used:

$$x = R_h \sinh\mu \sin\nu \cos\phi, \tag{2}$$
$$y = R_h \sinh\mu \sin\nu \sin\phi, \tag{3}$$
$$z = R_h \cosh\mu \cos\nu, \tag{4}$$

where, for convenience, we have defined the half-bond distance

$$R_h = \frac{1}{2}R \tag{5}$$

to avoid carrying various fractions in the equations. In equation (5), R is the internuclear distance, the two nuclei Z_A and Z_B being thus placed at $(0, 0, -R_h)$ and $(0, 0, R_h)$, respectively. The distances of a point from the two nuclei and from the origin can thereby be written as

$$r_A = R_h(\cosh\mu + \cos\nu), \tag{6}$$
$$r_B = R_h(\cosh\mu - \cos\nu), \tag{7}$$
$$r = R_h\sqrt{\cosh^2\mu + \cos^2\nu - 1}, \tag{8}$$

respectively, while the spherical polar angle $\cos\theta = z/r$ can be written as

$$\cos\theta = \frac{\cosh\mu\cos\nu}{\sqrt{\cosh^2\mu + \cos^2\nu - 1}}. \tag{9}$$

As was discussed in ref. 2, isosurfaces of μ approach spheres for large values of the coordinate. This can also be seen from equation (8): for large values of μ, the distance from the origin approaches

$$r \to R_h \cosh\mu, \tag{10}$$

the same limit is also achieved when $R \to 0$, in which case the usual spherical polar coordinate system is obtained.[9] Thus, by convention, the value of the practical infinity r_∞ is typically chosen in fully numerical diatomic calculations in the same way as in atomic calculations, that is, by specifying the radius of a large sphere centered at the origin, which encloses the system. The corresponding μ value can then be obtained as

$$\mu_\infty = \operatorname{arcosh}\frac{r_\infty}{R_h} = \operatorname{arcosh}\frac{2r_\infty}{R}. \tag{11}$$

Alternatively, since $\cosh\mu$ is large while μ is by definition non-negative, one can furthermore approximate

$$\cosh\mu = \frac{1}{2}\left(e^{\mu} + e^{-\mu}\right) \approx \frac{1}{2}e^{\mu} \tag{12}$$

which yields a simpler approximate form

$$\mu_{\infty} \approx \log\frac{4r_{\infty}}{R}. \tag{13}$$

Calculations in the curvilinear coordinate system defined by equations (2), (3) and (4) will require knowledge of the scale factors

$$h_i(\xi,\eta,\phi) = \sqrt{(\partial_i x)^2 + (\partial_i y)^2 + (\partial_i z)^2}. \tag{14}$$

These are straightforwardly obtained as

$$h_{\phi} = R_h \sinh\mu \sin\nu, \tag{15}$$

$$h_{\nu} = R_h \sqrt{\sinh^2\mu + \sin^2\nu}, \tag{16}$$

$$h_{\mu} = R_h \sqrt{\sinh^2\mu + \sin^2\nu}. \tag{17}$$

The volume element is then obtained as

$$\mathrm{d}V = h_{\phi}h_{\nu}h_{\mu}\mathrm{d}\phi\mathrm{d}\nu\mathrm{d}\mu \tag{18}$$

$$= R_h^3 \sinh\mu\sin\nu\left(\sinh^2\mu + \sin^2\nu\right)\mathrm{d}\phi\mathrm{d}\nu\mathrm{d}\mu \tag{19}$$

$$= R_h^3 \sinh\mu\sin\nu\left(\cosh^2\mu - \cos^2\nu\right)\mathrm{d}\phi\mathrm{d}\nu\mathrm{d}\mu. \tag{20}$$

Identifying the angular element of the spherical polar coordinate system

$$\mathrm{d}\Omega = \sin\nu\mathrm{d}\nu\mathrm{d}\phi, \tag{21}$$

over which the spherical harmonics are orthonormal, the volume element is obtained in the final form

$$\mathrm{d}V = R_h^3 \sinh\mu\left(\cosh^2\mu - \cos^2\nu\right)\mathrm{d}\mu\mathrm{d}\Omega. \tag{22}$$

Comparing equations (6), (7) and (22), it is seen that the volume element contains the factor $r_A r_B$, which is the reason for the good performance of the prolate spheroidal coordinate system. Nuclear attraction integrals are smooth and have no singularities, as the r_A^{-1} and r_B^{-1} terms arising from the attraction of the two nuclei are canceled by a factor in the volume element. In addition, as discussed in ref. 2, the presently used coordinate system is especially nice for fully numerical approaches, as exponential functions $\exp(-\zeta r_A)$ or $\exp(-\zeta r_B)$ turn to Gaussians in the (μ,ν,ϕ) coordinates near the nuclei, thereby lacking cups that would be difficult to represent numerically.

2.2 Basis set

As in atoms, in diatomic molecules orbitals block by the m quantum number:[3]

$$\psi_{nm}(\boldsymbol{r}) = \chi_{nm}(\mu,\nu)e^{im\phi}. \tag{23}$$

Thus, a basis set is adopted in the form

$$\chi_{nlm}(\mu,\nu,\phi) = B_n(\mu)Y_l^m(\nu,\phi) \tag{24}$$

where Y_l^m are complex spherical harmonics, and $B_n(\mu)$ are one-dimensional finite element basis functions, which are commonly known also as shape functions. The functions $B_n(\mu)$ are piece-wise polynomials that are non-zero only within a single *element* $\mu \in [\mu_{\mathrm{start}}, \mu_{\mathrm{end}}]$; see ref. 1 for more information on the approach. In analogy to the atomic case discussed in part I,[1] despite complex basis functions, all the matrices in HF

and DFT calculations end up being real – even in the presence of a parallel magnetic field [32] – unless special approaches are used. [33–38]

The angular parts of matrix elements in the basis defined by equation (24) can be evaluated in closed form, [4,39] and most matrix elements will vanish by symmetry, as will be seen later on in the manuscript. As in the atomic case, the same radial grid is used for all angular momentum channels, as it greatly simplifies the implementation; the total number of basis functions again being given by the number of radial functions times that of angular functions.

2.3 One-electron integrals

As the volume element includes a $\cos^2\nu$ factor, the angular basis set will not be orthonormal in contrast to the atomic case: in addition to the diagonal coupling from (l,m) to (l,m), the overlap matrix also includes couplings to $(l-2,m)$ and to $(l+2,m)$. As angular integrals over cosines will appear here and there, we define a cosine coupling coefficient as

$$\delta^{(n)}_{l_1 l_2} = \int \left(Y^0_{l_2}\right)^* (\nu,\phi) Y^0_{l_1}(\nu,\phi) \cos^n \nu \mathrm{d}\Omega, \tag{25}$$

where the case $n=0$ yields the Kronecker delta symbol $\delta_{l_1 l_2}$. The cosine factors encountered in the present work can be expanded in spherical harmonics as

$$\cos\nu = \frac{2}{3}\sqrt{3\pi}Y^0_1 \tag{26}$$

$$\cos^2\nu = \frac{2}{3}\sqrt{\pi}Y^0_0 + \frac{4}{15}\sqrt{5\pi}Y^0_2 \tag{27}$$

$$\cos^3\nu = \frac{2}{5}\sqrt{3\pi}Y^0_1 + \frac{4}{35}\sqrt{7\pi}Y^0_3 \tag{28}$$

$$\cos^4\nu = \frac{2}{5}\sqrt{\pi}Y^0_0 + \frac{8}{35}\sqrt{5\pi}Y^0_2 + \frac{16}{105}\sqrt{\pi}Y^0_4 \tag{29}$$

$$\cos^5\nu = \frac{2}{7}\sqrt{3\pi}Y^0_1 + \frac{8}{63}\sqrt{7\pi}Y^0_3 + \frac{16}{693}\sqrt{11\pi}Y^0_5 \tag{30}$$

and thus the values of $\delta^n_{l_1 l_2}$ can be evaluated easily from Gaunt coefficients

$$Y^{m_1}_{l_1}(\Omega) Y^{m_2}_{l_2}(\Omega) = \sum_{LM} G^{m_1 m_2, L}_{l_1 l_2, M} Y^M_L(\Omega) \tag{31}$$

as discussed in ref. 40. Note that we use an asymmetric definition for the Gaunt coefficient in equation (31), as discussed in part I of the present series. [1]

All the necessary Gaunt coefficients are precomputed and stored in memory at the start of the calculation. Note that unlike the atomic case, in which the angular expansion is always limited, the angular momentum l may attain large values in the partial wave expansion for diatomic molecules: for instance, the calculations on Cu_2 and CuLi in the present work used expansions up to $l=46$. Although elegant schemes for the sparse storage of Gaunt coefficient tables have been discussed in the literature, [41,42] in the present case only a small subset of m values is needed – from $m=0$ for σ orbitals to $m=\pm 3$ for φ orbitals – and so a simple dense cubic array storage scheme $[(l_1,m_1),(l_2,m_2);(L,M)]$ is sufficient for our work.

2.3.1 Overlap

Defining the radial integrals

$$I^{mn}_{ij} = \int B_i(\mu) B_j(\mu) \sinh^m\mu \cosh^n\mu \mathrm{d}\mu, \tag{32}$$

the overlap integral can be written as

$$S_{ij} = \int B_i(\mu) Y^*_{l_i m_i}(\mathbf{\Omega}) B_j(\mu) Y_{l_j m_j}(\mathbf{\Omega}) R_h^3 \sinh\mu \left(\cosh^2\mu - \cos^2\nu\right) \mathrm{d}\mu\mathrm{d}\Omega \tag{33}$$

$$= \left(R_h^3 I^{12}_{ij} \delta_{l_i,l_j} - R_h^3 I^{10}_{ij} \delta^{(2)}_{l_i,l_j}\right) \delta_{m_i,m_j}. \tag{34}$$

The radial integrals are computed using Gauss–Chebyshev quadrature as detailed in part I,[1] and integration over $\mu = [0, \infty)$ is again implied for brevity in the equations.

2.3.2 Kinetic energy

Also the kinetic energy is simple. The Laplacian is given by

$$\begin{aligned}
\nabla^2 f =& \frac{1}{h_\phi h_\nu h_\mu}\left[\frac{\partial}{\partial\mu}\left(\frac{h_\nu h_\phi}{h_\mu}\frac{\partial f}{\partial\mu}\right)+\frac{\partial}{\partial\nu}\left(\frac{h_\mu h_\phi}{h_\nu}\frac{\partial f}{\partial\nu}\right)+\frac{\partial}{\partial\phi}\left(\frac{h_\mu h_\nu}{h_\phi}\frac{\partial f}{\partial\phi}\right)\right] && (35)\\
=& \frac{\mathrm{d}\phi\mathrm{d}\nu\mathrm{d}\mu}{\mathrm{d}V}R_h\Bigg[\sin\nu\frac{\partial}{\partial\mu}\left(\sinh\mu\frac{\partial f}{\partial\mu}\right)+\sinh\mu\frac{\partial}{\partial\nu}\left(\sin\nu\frac{\partial f}{\partial\nu}\right)\\
&+\frac{\sinh^2\mu+\sin^2\nu}{\sinh\mu\sin\nu}\frac{\partial}{\partial\phi}\left(\frac{\partial f}{\partial\phi}\right)\Bigg], && (36)\\
=& \frac{1}{R_h^2\left(\sinh^2\mu+\sin^2\nu\right)}\left[\frac{1}{\sinh\mu}\left(\frac{\partial}{\partial\mu}\left(\sinh\mu\frac{\partial f}{\partial\mu}\right)\right)+\frac{1}{\sin\nu}\frac{\partial}{\partial\nu}\left(\sin\nu\frac{\partial f}{\partial\nu}\right)\right]\\
&+\frac{1}{R_h^2\sinh^2\mu\sin^2\nu}\frac{\partial^2 f}{\partial\phi^2} && (37)
\end{aligned}$$

in full agreement with Artemyev *et al.*[10] Knowing that the spherical harmonics satisfy

$$\begin{aligned}
\frac{\partial^2}{\partial\phi^2}Y_l^m(\cos\nu,\phi) =& -m^2 Y_l^m, && (38)\\
\left[\frac{1}{\sin\nu}\frac{\partial}{\partial\nu}\left(\sin\nu\frac{\partial}{\partial\nu}\right)-\frac{m^2}{\sin^2\nu}\right]Y_l^m(\cos\nu,\phi) =& -l(l+1)Y_l^m(\cos\nu,\phi), && (39)
\end{aligned}$$

the Laplacian (equation (37)) of a basis function yields

$$\begin{aligned}
\nabla^2\chi_j =& \frac{1}{R_h^2\left(\sinh^2\mu+\sin^2\nu\right)}\left[\frac{1}{\sinh\mu}\left(\frac{\partial}{\partial\mu}\left(\sinh\mu\frac{\partial B_j}{\partial\mu}\right)\right)Y_{l_j}^{m_j}\right.\\
&\left.-B_j(\mu)\left(l_j(l_j+1)+\frac{m_j^2}{\sinh^2\nu}\right)Y_{l_j}^{m_j}\right] && (40)
\end{aligned}$$

in agreement with McCullough.[39] Thus, the kinetic energy matrix element becomes

$$\begin{aligned}
T_{ij} =& \int\chi_i^*(\boldsymbol{r})\left(-\frac{1}{2}\nabla^2\right)\chi_j(\boldsymbol{r})\mathrm{d}^3 r && (41)\\
=& -\frac{1}{2}\int R_h B_i(\mu)\left(\frac{\partial}{\partial\mu}\left(\sinh\mu\frac{\partial B_j}{\partial\mu}\right)\right)\int\left(Y_{l_i}^{m_i}\right)^* Y_{l_j}^{m_j}\mathrm{d}\mu\mathrm{d}\Omega\\
&+\frac{1}{2}\int R_h B_i(\mu)\left[l_j(l_j+1)\sinh\mu+\frac{m_j^2}{\sinh\mu}\right]d\mu\int\left(Y_{l_i}^{m_i}\right)^* Y_{l_j}^{m_j}\mathrm{d}\Omega. && (42)
\end{aligned}$$

Finally, the first term can be symmetrized by invoking integration by parts, as in the atomic case discussed in part I,[1] yielding the kinetic energy matrix elements in the final form

$$T_{ij} = \frac{R_h}{2}\left[D_{i,j}+l_j(l_j+1)I_{1,2}^{10}+m_j^2 I_{i,j}^{-1,0}\right]\delta_{l_i,l_j}\delta_{m_i,m_j}, \quad (43)$$

where we have defined the radial integral

$$D_{1,2} = \int\sinh\mu\frac{\partial B_1}{\partial\mu}\frac{\partial B_2}{\partial\mu}\mathrm{d}\mu. \quad (44)$$

The examination of equation (42) shows that the kinetic energy density diverges for $\mu \to 0$ for $m \neq 0$. This means that non-σ states must vanish at $\mu = 0$

$$\psi_m(\mu = 0, \nu) = 0, m \neq 0. \tag{45}$$

Unlike the atomic case discussed in part I, [1] the used radial basis set must then depend on the value m. However, equation (45) can be satisfied in the finite element implementation as described in ref. 1 by removing the first shape function of the first radial element for basis functions with $m \neq 0$, which is easily done in the C++ program.

2.3.3 Nuclear attraction

As was stated above in section 2.1, the nuclear attraction integrals become easy for quadrature in the prolate spheroidal coordinate system, as the singularities at the nuclei are canceled out by factors in the volume element. The nuclear attraction integral is

$$V_{ij} = \int \chi_i^*(\boldsymbol{r}) \left(-\frac{Z_A}{r_A} - \frac{Z_B}{r_B} \right) \chi_2(\boldsymbol{r}) \mathrm{d}^3 r \tag{46}$$

$$= - R_h^2 \int \chi_i^*(\boldsymbol{r}) \left[(Z_A + Z_B) \cosh\mu + (Z_B - Z_A) \cos\nu \right] \chi_j(\boldsymbol{r}) \sinh\mu \mathrm{d}\mu \mathrm{d}\Omega \tag{47}$$

from which the integral is obtained in final form as

$$V_{ij} = - R_h^2 \left(Z_A + Z_B \right) I_{i,j}^{11} \delta_{l_i,l_j} \delta_{m_i,m_j} - R_h^2 \left(Z_B - Z_A \right) I_{i,j}^{10} \delta_{l_i,l_j}^{(1)} \delta_{m_i,m_j}. \tag{48}$$

2.3.4 Radial moments

Radial moments of the density about the nuclei can be calculated using

$$r_{A/B;ij}^{-1} = R_h^2 \left(I_{i,j}^{11} \delta_{l_i,l_j} \mp I_{i,j}^{10} \delta_{l_i,l_j}^{(1)} \right) \delta_{m_i,m_j} \tag{49}$$

and

$$r_{A/B} = R_h(\cosh\mu \pm \cos\nu) \tag{50}$$

$$r_{A/B}^2 = R_h(\cosh^2\mu \pm 2\cosh\mu\cos\nu + \cos^2\nu) \tag{51}$$

$$r_{A/B}^3 = R_h(\cosh^3\mu \pm 3\cosh^2\mu\cos\nu + 3\cosh\mu\cos^2\nu \pm \cos^3\nu) \tag{52}$$

from which

$$\left\langle r_{A/B} \right\rangle_{ij} = R_h^4 \left[I_{i,j}^{13} \delta_{l_i,l_j} \pm I_{i,j}^{12} \delta_{l_i,l_j}^{(1)} - I_{i,j}^{11} \delta_{l_i,l_j}^{(2)} \mp I_{i,j}^{10} \delta_{l_i,l_j}^{(3)} \right] \delta_{m_i,m_j} \tag{53}$$

$$\left\langle r_{A/B} \right\rangle_{ij}^2 = R_h^5 \left[I_{i,j}^{14} \delta_{l_i,l_j} \pm 2 I_{i,j}^{13} \delta_{l_i,l_j}^{(1)} \mp 2 I_{i,j}^{11} \delta_{l_i,l_j}^{(3)} - I_{i,j}^{10} \delta_{l_i,l_j}^{(4)} \right] \delta_{m_i,m_j} \tag{54}$$

$$\left\langle r_{A/B} \right\rangle_{ij}^3 = R_h^6 \left[I_{i,j}^{15} \delta_{l_i,l_j} \pm 3 I_{i,j}^{14} \delta_{l_i,l_j}^{(1)} + 2 I_{i,j}^{13} \delta_{l_i,l_j}^{(2)} \mp 2 I_{i,j}^{12} \delta_{l_i,l_j}^{(3)} - 3 I_{i,j}^{11} \delta_{l_i,l_j}^{(4)} \mp I_{i,j}^{10} \delta_{l_i,l_j}^{(5)} \right] \delta_{m_i,m_j} \tag{55}$$

In equations (49) to (55), the upper sign corresponds to placing the origin at the left-hand atom A at $z = -R_h$, while the lower sign corresponds to placing the origin at the right-hand atom B at $z = R_h$. The radial expectation value with respect to the origin at the geometrical center of the molecule is

$$\left\langle r^2 \right\rangle_{ij} = R_h^5 \left[\left(I_{i,j}^{14} - I_{i,j}^{12} \right) \delta_{l_i,l_j} + I_{i,j}^{10} \left(\delta_{l_i,l_j}^{(2)} - \delta_{l_i,l_j}^{(4)} \right) \right] \delta_{m_i,m_j}. \tag{56}$$

2.3.5 Electric field

The orbitals block by m even in the presence of an electric field parallel to the molecular bond, *i.e.* in the z direction; the analogous case for magnetic fields is discussed in ref. 32. The z component of the dipole

operator is given by

$$\mu_{z;ij} = \int \chi_i^*(\boldsymbol{r}) z \chi_j(\boldsymbol{r}) \mathrm{d}V \tag{57}$$

$$= \int B_i(\mu) B_j(\mu) R_h \cosh\mu \cos\nu \cdot R_h^3 \sinh\mu \left(\cosh^2\mu - \cos^2\nu\right) \mathrm{d}\mu \mathrm{d}\Omega \left(Y_{l_i}^{m_i}\right)^* Y_{l_j}^{m_j} \tag{58}$$

$$= R_h^4 \left[I_{i,j}^{13} \delta_{l_i,l_j}^{(1)} - I_{i,j}^{11} \delta_{l_i,l_j}^{(3)} \right] \delta_{m_i,m_j}. \tag{59}$$

The zz component of the quadrupole operator is

$$\Theta_{zz} = \frac{1}{2}\left(3z^2 - r^2\right) = \frac{R_h^2}{2}\left[3\cosh^2\mu\cos^2\nu - \cosh^2\mu - \cos^2\nu + 1\right] \tag{60}$$

which has the matrix element

$$\Theta_{zz;ij} = \int \chi_i^*(\boldsymbol{r}) \Theta_{zz} \chi_j(\boldsymbol{r}) \mathrm{d}^3 r \tag{61}$$

$$= \frac{R_h^5}{2}\left[\left(I_{ij}^{12} - I_{ij}^{14}\right) \delta_{l_i,l_j} + \left(3I_{ij}^{14} - I_{ij}^{10}\right) \delta_{l_i,l_j}^{(2)} + \left(I_{ij}^{10} - 3I_{ij}^{12}\right) \delta_{l_i,l_j}^{(4)} \right] \delta_{m_i,m_j}. \tag{62}$$

The nuclear contributions to the electric dipole and quadrupole moments are

$$\mu_z^{\mathrm{nuc}} = R_h(Z_2 - Z_1), \tag{63}$$

$$\Theta_{zz}^{\mathrm{nuc}} = R_h^2\left(Z_1 + Z_2\right). \tag{64}$$

Equations (57) and (64) are with respect to the origin; moments with respect to other origins such as the center of mass or center of charge are deferred to future work.

2.4 Two-electron integrals

The two-electron integrals

$$(ij|kl) = \int \frac{\chi_i(\boldsymbol{r}) \chi_j^*(\boldsymbol{r}) \chi_k(\boldsymbol{r}') \chi_l^*(\boldsymbol{r}')}{|\boldsymbol{r} - \boldsymbol{r}'|} \mathrm{d}^3 r \mathrm{d}^3 r' \tag{65}$$

can be readily evaluated with the help of the Neumann expansion, as was originally pointed out by McCullough;[4,39] the same approach has also been used in refs. 10 and 43, for example. As has been discussed by Ruedenberg (equation 4.13 in reference 9), the Neumann expansion of r_{12}^{-1} is given by

$$\frac{1}{r_{12}} = \frac{4\pi}{R_h} \sum_{L=0}^{\infty} \sum_{M=-L}^{L} (-1)^M \frac{(L - |M|)!}{(L + |M|)!} P_L^{|M|}(\cosh\mu_<) Q_L^{|M|}(\cosh\mu_>) Y_L^M(\Omega_1) \left(Y_L^M(\Omega_2)\right)^*, \tag{66}$$

where P_L^M, Q_L^M are associated Legendre functions of the first and second kind, respectively. Note that equation (66) contains Legendre functions in two places: first, explicitly shown with the argument $\cosh\mu \geq 1$, and second, inside the spherical harmonics with the more familiar branch $|\cos\nu| \leq 1$. The evaluation of the functions for the former case is not as well known, but can be readily accomplished with software libraries described in the literature.[44–46] In the present work, the library by Schneider and coworkers is used for the evaluation of the Legendre functions in $\cosh\mu$.[45,46]

The Neumann expansion is analogous to the Laplace expansion that was used for atomic calculations in part I,[1] with $P_L^{|M|}(\mu)$ taking the place of r^{-L-1} in the large-radius integral, and $Q_L^{|M|}$ taking the place of r^L in the small-radius integral. Analogously to the atomic case, $P_L^{|M|}(\cosh\mu)$ are regular at $\mu = 0$ but diverge as $\mu \to \infty$, while $Q_L^{|M|}(\cosh\mu)$ diverge at $\mu = 0$ but go to zero for $\mu \to \infty$. Note, however, that in contrast to the atomic case where the integrand only depends on L, the diatomic integrals also depend on M, indicating a more costly approach: even though the usual spherical polar coordinate system is obtained by letting $R \to 0$ in a diatomic calculation,[9] the diatomic two-electron interactions still require more work than the atomic calculations presented in part I.[1]

Substituting the Neumann expansion (equation (66)) into equation (65) yields

$$\begin{aligned}(ij|kl) =&4\pi R_h^5 \sum_{L=0}^{\infty} \sum_{M=-L}^{L} (-1)^M \frac{(L-|M|)!}{(L+|M|)!} \int \mathrm{d}\mu_1 \mathrm{d}\mu_2 \mathrm{d}\Omega_1 \mathrm{d}\Omega_2 P_L^{|M|}(\cosh\mu_<) Q_L^{|M|}(\cosh\mu_>) \\ &\int \left(\cosh^2\mu_1 - \cos^2\nu_1\right) \sinh\mu_1 B_i(\mu_1) B_j(\mu_1) Y_{l_i}^{m_i}(\Omega_1) \left(Y_{l_j}^{m_j}(\Omega_1)\right)^* Y_L^M(\Omega_1) \\ &\int \left(\cosh^2\mu_2 - \cos^2\nu_2\right) \sinh\mu_2 B_k(\mu_2) B_l(\mu_2) Y_{l_k}^{m_k}(\Omega_2) \left(Y_{l_l}^{m_l}(\Omega_2)\right)^* \left(Y_L^M(\Omega_2)\right)^*. \end{aligned} \tag{67}$$

From here, we see that we must have

$$m_j - m_i = M = m_k - m_l \tag{68}$$

in order for the integral to be non-zero; the very same condition was obtained also in the atomic case in ref. 1. Furthermore, the angular momentum algebra places limits on L as in the atomic case as

$$L_{\min} \leq L \leq L_{\max}. \tag{69}$$

However, the cosine factors in equation (67) extend the range of the coupled angular momentum by two in each direction compared to the atomic case, yielding

$$L_{\min} = \max\{|l_i - l_j|, |l_k - l_l|\} - 2, \tag{70}$$

$$L_{\max} = \min\{|l_i + l_j|, |l_k + l_l|\} + 2, \tag{71}$$

again signifiying more work than in an atomic calculation. The final condition for the integral to be nonzero is that Y_L^M must exist, which gives

$$L_{\min} \geq |M|. \tag{72}$$

Equations (68) to (72) truncate the infinite sum in equation (67) to a finite number of terms:

$$\begin{aligned}(ij|kl) = \sum_{L=L_{\min}}^{L_{\max}} \Bigg[& I_{ij,kl}^{22,L|M|} G_{Ll_i,m_j}^{Mm_i,l_j} G_{Ll_l,m_k}^{Mm_l,l_k} - I_{ij,kl}^{02,L|M|} \tilde{G}_{Ll_i,m_j}^{Mm_i,l_j} G_{Ll_l,m_k}^{Mm_l,l_k} \\ & - I_{ij,kl}^{20,L|M|} G_{Ll_i,m_j}^{Mm_i,l_j} \tilde{G}_{Ll_l,m_k}^{Mm_l,l_k} + I_{ij,kl}^{00,L|M|} \tilde{G}_{Ll_i,m_j}^{Mm_i,l_j} \tilde{G}_{Ll_l,m_k}^{Mm_l,l_k} \Bigg], \end{aligned} \tag{73}$$

where M, $L_{\min}$, $L_{\max}$ and are given by equations (68), (70) and (71), respectively, $I_{ij,kl}^{\alpha\beta,L|M|}$ are primitive integrals, and we have defined a modified Gaunt coefficient as

$$\tilde{G}_{Ll_i,m_j}^{Mm_i,l_j} = \int \cos^2\nu Y_{l_i}^{m_i}(\Omega) \left(Y_{l_j}^{m_j}\right)^*(\Omega) Y_L^M(\Omega) \,\mathrm{d}\Omega \tag{74}$$

to account for the $\cos^2\nu$ terms. By employing equations (27) and (31), the modified Gaunt coefficient in equation (74) can be written in terms of the usual Gaunt coefficients as

$$\tilde{G}_{Ll_i,m_j}^{Mm_i,l_j} = \frac{2\sqrt{\pi}}{3} G_{L0,M}^{M0,L} G_{Ll_i,m_j}^{Mm_i,l_j} + \frac{4}{15}\sqrt{5\pi} \sum_{L'=L-2}^{L+2} G_{L2,M}^{M0,L'} G_{L'l_i,m_j}^{Mm_i,l_j}. \tag{75}$$

2.4.1 Primitive integrals

The primitive integrals used in equation (73) are defined as

$$\begin{aligned} I_{ij,kl}^{\alpha\beta,L|M|} =&4\pi R_h^5 (-1)^{|M|} \frac{(L-|M|)!}{(L+|M|)!} \int \cosh^\alpha\mu_1 \sinh\mu_1 \cosh^\beta\mu_2 \sinh\mu_2 \\ &\times B_i(\mu_1) B_j(\mu_1) B_k(\mu_2) B_l(\mu_2) P_L^{|M|}(\cosh\mu_<) Q_L^{|M|}(\cosh\mu_>) \mathrm{d}\mu_1 \mathrm{d}\mu_2 \end{aligned} \tag{76}$$

which alike the atomic case can be specialized into two cases: one where all four functions are within the same element, and another where i and j are in one element and k and l are in another. Note that the expression corresponding to equation (76) of Artemyev *et al.* (equation 32 in reference 10) is missing the $\cosh^\alpha \mu_1 \sinh \mu_1 \cosh^\beta \mu_2 \sinh \mu_2$ factors arising from the volume elements.

As can be seen from equation (73), four sets of primitive integrals corresponding to $(\alpha\beta) = (00)$, (02), (20), (22) are needed, again increasing the amount of work compared to an atomic calculation, with the possible values for L and M ranging from $L = 0, \ldots, 2\,(l_{\max} + 1)$ and $|M| = 0, \ldots, 2m_{\max}$, where $l_{\max}$ and $m_{\max}$ are the largest values of l and m in the basis set.

Like in the atomic case, most of the two-electron integrals in big calculations arise from interelement integrals, which are written in the factorizable form

$$\begin{aligned} I_{ij,kl}^{\alpha\beta,L|M|} =& 4\pi R_h^5 (-1)^{|M|} \frac{(L-|M|)!}{(L+|M|)!} \left[\int_{\mu_1^{\min}}^{\mu_1^{\max}} \cosh^\alpha \mu_1 \sinh \mu_1 Q_L^{|M|}(\cosh \mu_1) B_i(\mu_1) B_j(\mu_1) \mathrm{d}\mu_1 \right] \\ & \times \left[\int_{\mu_2^{\min}}^{\mu_2^{\max}} \cosh^\beta \mu_2 \sinh \mu_2 B_k(\mu_2) B_l(\mu_2) P_L^{|M|}(\cosh \mu_2) \mathrm{d}\mu_2 \right], \end{aligned} \tag{77}$$

where we have assumed that the element containing ij is farther from the origin than the one containing kl. As in the atomic case, the factorization in equation (77) can be used in the Coulomb and exchange matrix algorithms. Also alike the atomic case, the intraelement integrals are evaluated in three steps:

$$\phi_{kl}^{\beta,L|M|}(\mu) = \int_0^\mu \mathrm{d}\mu' \cosh^\beta \mu' \sinh \mu' B_k(\mu') B_l(\mu') P_L^{|M|}(\cosh \mu'), \tag{78}$$

$$i_{ij,kl}^{\alpha\beta,L|M|} = \int_0^\infty \mathrm{d}\mu \cosh^\alpha \mu \sinh \mu B_i(\mu) B_j(\mu) Q_L^{|M|}(\cosh \mu) \phi_{kl}^{\beta,L|M|}(\mu), \tag{79}$$

$$I_{ij,kl}^{\alpha\beta,L|M|} = i_{ij,kl}^{\alpha\beta,L|M|} + i_{kl,ij}^{\beta\alpha,L|M|}, \tag{80}$$

where equation (78) is computed in slices in analogy to the atomic treatment. Note that in the last step, *i.e.* in equation (80), both $ij \leftrightarrow kl$ and $\alpha \leftrightarrow \beta$ are interchanged.

2.4.2 Coulomb matrix

The evaluation of Coulomb and exchange matrices can be sped up significantly by employing the same techniques as in the atomic case of part I.[1] This has also been recognized early on by McCullough.[39] The Coulomb matrix is given by

$$J_{ij} = \sum_{kl} (ij|kl) P_{kl}. \tag{81}$$

Substituting the expression for the two-electron integrals (equation (73)) into equation (81) one obtains

$$\begin{aligned} J_{ij} = \sum_{L_{\min}}^{L_{\max}} \Bigg[& I_{ij,kl}^{22,L|M|} P_{kl} G_{Ll_i,m_j}^{Mm_i,l_j} G_{Ll_l,m_k}^{Mm_l,l_k} - I_{ij,kl}^{02,L|M|} P_{kl} \tilde{G}_{Ll_i,m_j}^{Mm_i,l_j} G_{Ll_l,m_k}^{Mm_l,l_k} \\ & - I_{ij,kl}^{20,L|M|} P_{kl} G_{Ll_i,m_j}^{Mm_i,l_j} \tilde{G}_{Ll_l,m_k}^{Mm_l,l_k} + I_{ij,kl}^{00,L|M|} P_{kl} \tilde{G}_{Ll_i,m_j}^{Mm_i,l_j} \tilde{G}_{Ll_l,m_k}^{Mm_l,l_k} \Bigg] \end{aligned} \tag{82}$$

where M is defined by the constraint in equation (68), and $L_{\min}$ and $L_{\max}$ are defined by equations (70) to (72). Because the primitive integrals $I_{ij,kl}^{\alpha\beta,L|M|}$ only depend on the radial part and the compound index $L|M|$, one can form the Coulomb matrix efficiently in three steps, analogously to the atomic calculations discussed in part I.[1] The key here is to form radial helper matrices by summing over the angular contributions as

$$P_{kl}^{L|M|} = \sum_{kl} G_{Ll_l,m_k}^{Mm_l,l_k} P_{kl}, \tag{83}$$

$$\tilde{P}_{kl}^{L|M|} = \sum_{kl} \tilde{G}_{Ll_l,m_k}^{Mm_l,l_k} P_{kl}, \tag{84}$$

contract them with the primitive integrals to yield radial-only Coulomb matrices

$$J_{ij}^{L|M|} = \sum_{kl} I_{ij,kl}^{22,L|M|} P_{kl}^{L|M|} - \sum_{kl} I_{ij,kl}^{20,L|M|} \tilde{P}_{kl}^{L|M|} \tag{85}$$

$$\tilde{J}_{ij}^{L|M|} = \sum_{kl} I_{ij,kl}^{00,L|M|} \tilde{P}_{kl}^{L|M|} - \sum_{kl} I_{ij,kl}^{02,L|M|} P_{kl}^{L|M|} \tag{86}$$

and last, unroll the radial-only Coulomb matrices into the full Coulomb matrix as

$$J_{ij} = J_{ij}^{L|M|} G_{Ll_i,m_j}^{Mm_i,l_j} + \tilde{J}_{ij}^{L|M|} \tilde{G}_{Ll_i,m_j}^{Mm_i,l_j}. \tag{87}$$

The factorization of the interelement integrals can be used in equations (85) and (86) to yield further speed improvements, whereas the contraction of intraelement integrals can be done by matrix-vector multiplication.

2.4.3 Exchange matrix

For the exchange we have

$$K_{jk}^{\sigma} = \sum_{il} (ij|kl) P_{il}^{\sigma} \tag{88}$$

which can also be made more efficient by summing over the angular parts of il. However, while a single expansion over L and $|M|$ sufficed for the Coulomb matrix, in the case of the exchange matrix, the expansion has to be performed for all jk, making the calculation significantly more expensive. As in the atomic case, the factorization of the interelement integrals can be used to make the algorithm scale better, while the intraelement contractions can be made faster by storing a permuted set of the integrals in memory, allowing the use of matrix-vector products.

2.5 DFT

The implementation of DFT is exactly the same as in the atomic case discussed in part I;[1] only the scale factors given in equations (15) to (17) are different. As in the atomic case, Gauss–Chebyshev quadrature is used in the ν direction, whereas an equidistant grid is used for ϕ. We have chosen $n_\nu = 4l_{\max} + 12$ and $n_\phi = 4m_{\max} + 5$ as the default values for diatomic calculations, where the two extra points in the ν quadrature compared to the atomic calculations have been added due to the $\cos^2 \nu$ factor in the volume element.

As was discussed for the atomic case in part I,[1] popular functionals such as CAM-B3LYP;[47] the Minnesota functionals M11,[48] N12-SX,[49] and MN12-SX;[49] and the Head-Gordon group's ωB97,[50] ωB97X,[50], ωB97X-V,[51] and ωB97M-V[52] functionals employ a range-decomposed Coulomb interaction[53]

$$\frac{1}{r_{12}} = \frac{\phi_{\mathrm{sr}}(r_{12};\omega)}{r_{12}} + \frac{1 - \phi_{\mathrm{sr}}(r_{12};\omega)}{r_{12}}, \tag{89}$$

in the exchange contribution, where the weight function is chosen as

$$\phi_{\mathrm{sr}}(r;\omega) = \mathrm{erfc}(r;\omega). \tag{90}$$

Implementing the aforementioned functionals in the present approach would require a Neumann expansion for equations (89) and (90) alike equation (66). As was mentioned in part I,[1] we are not aware of suitable expansions even for the simpler atomic case, but such expansions could be pursued in future work.

2.6 Integral couplings

Having formulated expressions for all the integrals, it is useful to study the couplings between the different angular blocks that have been summarized in table 1. In contrast to the atomic case, where all one-electron operators were diagonal in l in the absence of electric fields, now only the kinetic energy is diagonal, while everything else contains couplings between different l blocks in the basis set.

Matrix type	Value of l' coupling to l	Radial elements dependent on l
Kinetic	l	yes
Nuclear attraction	l, $l \pm 1$	no
Overlap	l, $l \pm 2$	no
Dipole	$l \pm 1$, $l \pm 3$	no
Quadrupole	l, $l \pm 2$, $l \pm 4$	no

Table 1: One-electron integral couplings.

The wave function for one-electron systems in the absence of electromagnetic fields is determined by the overlap, kinetic and nuclear attraction matrices. Although the overlap and nuclear attraction matrices contain couplings between the various l channels in the basis set, their matrix elements are independent of l: the $(l = 0, m; l = 0, m)$ block has the same elements as the $(l = 2, m; l = 2, m)$ block. Also the dipole and quadrupole matrix elements are independent of l.

In contrast, while the kinetic energy operator does not couple different values of l, its matrix elements are l-dependent, higher l blocks carrying higher kinetic energy, as seen from equation (43). This can be understood by the form of the basis set: higher values of l correspond to variation at finer scales, which carry higher kinetic energy. Although the two-electron integrals also carry dependence on the angular momentum, this analysis shows that the convergence of a calculation is mainly determined by the kinetic energy.

2.7 Choice of basis set

The CBS limit can be achieved in principle by systematically expanding the basis set towards larger and larger values of l for all the values of m included in the basis set. In addition to the angular basis set, one must also converge the radial basis set, which implies another truncation parameter. Although it is very well possible to converge a calculation to the basis set limit by running a large number of SCF calculations at increasing numbers of partial waves and radial elements, this approach quickly becomes laborious, not to mention overtly costly for heavier systems. Furthermore, as the coordinate system depends on the bond length, in principle the basis set should be converged separately at each geometry for every system.

The geometry dependence of the basis set requirements is easy to understand by the following argument. Take a diatomic molecule with nuclei Z_A and Z_B separated by R. As has been discussed above and in ref. 9, letting $R \to 0$, the prolate spheroidal coordinate system approaches the spherical polar coordinate system. This means that the diatomic calculation will approach an atomic one for the compound nucleus $Z = Z_A + Z_B$. The angular expansion in atomic calculations is extremely compact, as discussed in the first part of this series:[1] for instance, the exact HF ground state of all atoms from hydrogen to calcium is achievable with just four angular functions – Y_0^0, Y_1^{-1}, Y_1^0, and Y_1^{+1} – barring symmetry breaking effects. However, while the angular expansion becomes more compact when $R \to 0$, a heavier atom is also obtained at this limit, meaning that a larger radial grid must be employed. Thus, in order to reproduce potential energy surfaces, the radial grid should be converged at the *smallest* internuclear distance, whereas the angular grid should be converged at the *largest* internuclear distance.

Still, perhaps the worst feature of the naïve approach of running SCF calculations with larger and larger basis sets is the lack of estimates for the accuracy of any single calculation. The utility of the present approach would be greatly increased were there a way to easily choose a basis set for a given nuclear geometry with some degree of control over the resulting accuracy. The radial and the angular grids should be chosen in as balanced a way as possible to yield the best possible accuracy with the least number of basis functions, while minimizing the number of costly SCF calculations.

It is easy to see that the partial wave expansion should **not** be the same for all values of m: the deepest and most compact orbitals are the $1s$ core orbitals, which yield σ orbitals in the diatomic case. Atomic p orbitals yield two π orbitals ($m = \pm 1$) and one σ orbital; atomic d orbitals yield two δ ($m = \pm 2$) and π ($m = \pm 1$) orbitals and one σ orbital; and atomic f orbitals yield two φ ($m = \pm 3$), δ ($m = \pm 2$), and π ($m = \pm 1$) orbitals and one σ orbital, all of which are less compact the $1s$ σ orbital. Because higher values of l correspond to finer spatial resolution, it is obvious that the number of partial waves should be highest for the σ orbitals, and decrease in increasing $|m|$; this is also evident from the divergent $m^2/\sinh\mu$ term

in the kinetic energy, see equations (42) and (43). Thus, significant savings in the necessary number of basis functions can be expected by the use of a non-uniform angular grid, at no cost to the accuracy of the calculation. Unfortunately, decoupling the number of partial waves in every $|m|$ channel introduces further parameters that need to be optimized, as instead of a global cutoff value $l_{\max}$ one now has to optimize the partial wave cutoffs $l_{|m|}$ for $|m| = \sigma, \pi, \delta, \varphi$ in unison.

It is imaginable that an adaptive approach could be formulated for the choice of the basis set. The determination of the radial grid would be analogous to the atomic case, for which for both h-adaptive[54] and p-adaptive[55,56] approaches have been presented in the literature, while the sufficiency of the angular grid could be determined by determining the orbital gradient for rotations into angular functions not included in the current basis set. However, unless the occupations in each $|m|$ channel are predetermined, the use of the Aufbau principle in the SCF calculation may result in incorrect occupations if the angular basis set $l_{|m|}$ is unbalanced. For instance, the use of an insufficiently large l_π value may result in π orbital energies that are much too high, leading to σ orbitals being occupied by the Aufbau principle, instead. It is thus apparent that the adaptive basis set should be determined for a preset number of orbitals in each $|m|$ channel, but this would then require additional user interaction.

Instead of using an adaptive approach relying on SCF calculations as described above, we have found a simple and elegant solution to the problem of basis set selection via a single-particle proxy approach. Because higher l values express smaller and smaller details in the wave function – especially close to the nuclei – it makes sense to simply study the convergence of the wave function close to the nucleus, which can be approximated by the one-electron part of the Hamiltonian operator, *i.e.* the core Hamiltonian. In analogy to completeness-optimization,[57,58] both the radial and the angular basis set can be determined for any system at any geometry by studying the convergence of a proxy for the molecular energy

$$E^{\text{proxy}} = \sum_{i \text{ occ}} \epsilon_i^{\text{core}} \tag{91}$$

upon the addition of more radial elements or partial waves, where ϵ_i^{core} are the eigenvalues of the core Hamiltonian $\boldsymbol{H}_0 = \boldsymbol{T} + \boldsymbol{V}$. In order to maintain a balanced description, the addition trials increase the number of radial elements or partial waves by two, as in homonuclear systems the orbitals block by gerade/ungerade parity, which correspond to even/odd-numbered partial waves. As orbitals for $m = \pm|m|$ are fully degenerate for the core Hamiltonian, it suffices to only consider the states with $m \geq 0$ in the optimization.

The proxy corresponds to the one-electron part of the HF or DFT energy, and differs from the full energy by the interactions of the electrons. These omitted interactions extend the orbitals near the core, implying that the proxy may overestimate the necessary number of partial waves for the description of the wave function at an estimated accuracy Δ. Note that although hydrogenic orbitals (eigenfunctions of $\boldsymbol{H}_0$) are notoriously bad for chemistry, as they are typically both too compact due to the neglect of electronic repulsion effects, as well as quickly become too diffuse to yield needed flexibility in the molecular core and valence regions,[59] this is not a problem in the present approach as a predetermined r_∞ poses limits on the diffuseness of the orbitals, and as the dimension of the basis is not affected by the diagonalization of the core Hamiltonian. For more discussion on the core guess and for an alternative one-electron guess that could also be used as a proxy for basis set completeness, see ref. 60.

Importantly, unlike an SCF based procedure for the adaptive formation of the fully numerical basis set, the optimization of equation (91) requires no solution of the SCF equations, and is thereby fast to calculate; moreover, the m channels are fully decoupled so the $l_{|m|}$ values can be optimized separately. Furthermore, the number of occupied orbitals in each m channel can be chosen for any system simply by considering the blocks of the periodic table in which the nuclei in the calculation reside. Omitting the spin factor, in analogy to our earlier work with completeness-optimized basis sets[61,62] we choose the number of occupied proxy orbitals to cover the whole block in the periodic table. That is, the number of occupied orbitals in each m channel is determined by counting the number of occupied shells in the individual atom, and adding 1σ for s shells, $1\sigma1\pi$ for p shells, $1\sigma1\pi1\delta$ for d shells and $1\sigma1\pi1\delta1\varphi$ for f shells. For clarity, the whole completeness-optimization procedure is shown step by step in Algorithm 1.

Despite the differences between the proxy and the true HF / DFT energy, we will demonstrate later in the manuscript that the error in the SCF energy is similar to the estimate given by the proxy energy. To our knowledge, this is the first time a non-uniform, truncated angular basis set has been used in the literature. Note especially that McCullough's approach[39] used an $l_{\max}$ value *increasing* in m as $l_m = l_{\max} + |m|$ to

Algorithm 1 Formation of the diatomic basis set by the use of completeness-optimization for the proxy energy.

0. Specify the molecule (Z_A, Z_B, R) as well as the wanted accuracy ϵ.

1. Calculate the number of orbitals in each m channel, based on the blocks of the periodic table the atoms Z_A and Z_B belong to, as described in the main text. For instance, Sc has 4 s shells, 2 p shells, and 1 d shell; this means adding $4+2+1=7$ σ orbitals, 3 π_{+1} and π_{-1} orbitals, and 1 δ_{+2} and δ_{-2} orbitals for a single Sc atom.

2. Initialize the radial and angular basis sets: set the number of radial elements to $N_{\text{elem}} = 1$, and the partial wave cutoff in each channel to $l_m = |m|$.

3. Converge radial and angular basis sets for each channel $m \geq 0$, by looping down from the largest $|m|$ to 0.

   (a) Calculate the current value E_{cur} for the proxy energy, equation (91), by solving the hydrogenic orbitals and energies for the molecule (Z_A, Z_B, R) in the current fully numerical basis set.

   (b) Add more elements to the radial basis, $N_{\text{elem}} \to N_{\text{elem}} + 2$, and use equation (91) to calculate the resulting radial trial proxy energy E_{rad}.

   (c) Add more partial waves to the m channel, $l_m \to l_m + 2$, and use equation (91) to calculate the resulting angular trial proxy energy E_{ang}.

   (d) Calculate the angular and radial energy lowerings $\Delta E_{\text{ang}} = E_{\text{cur}} - E_{\text{ang}} \geq 0$ and $\Delta E_{\text{rad}} = E_{\text{rad}} - E_{\text{ang}} \geq 0$.

   (e) If $\Delta E_{\text{rad}} \geq \Delta E_{\text{ang}}$ and $\Delta E_{\text{rad}} \geq \epsilon$, set $N_{\text{elem}} \to N_{\text{elem}} + 2$ and go back to step 3a.

   (f) If $\Delta E_{\text{ang}} > \Delta E_{\text{rad}}$ and $\Delta E_{\text{ang}} \geq \epsilon$, set $l_m \to l_m + 2$ and go back to step 3a.

   (g) Otherwise, the wanted accuracy ϵ has been reached for the m channel; continue with the next m value.

4. Set the angular basis for $m = -|m|$ to that for $m = +|m|$: $l_{-|m|} = l_{|m|}$ for $m > 0$.

maintain the same number of partial waves in every m channel, whereas our results show that a rapidly decreasing l_m is sufficient to yield fast convergence to the CBS limit, bestowing significant speedups for the algorithm.

3 Computational details

The equations presented of section §2 have been implemented in the C++ language. The Armadillo library has been used for all matrix algebra,[63,64] using efficient basic linear algebra subroutine (BLAS) libraries for the matrix operations. The program is parallellized with OpenMP pragmas.

The one-electron and primitive two-electron integrals are precomputed and stored in memory at the beginning of the calculation. $5N_p$ points are used for radial integrals; this should suffice even for the highly non-linear integrals in DFT. The storage requirements for the integrals are small, because only the auxiliary integrals are stored instead of as instead of the full two-electron integral tensor. Also, only the intraelement auxiliary integrals are stored as full rank-4 tensors, while the interelement integrals are used in factorized form that allows for faster formation of the Coulomb and exchange matrices.

Exchange-correlation functionals are evaluated with the Libxc library.[14] Unless specified otherwise, SCF calculations are initialized with the core guess, *i.e.* eigenvectors of $\boldsymbol{H}_0 = \boldsymbol{T} + \boldsymbol{V}$, and the Aufbau principle is employed. A combination of the DIIS and ADIIS accelerators is used in the SCF procedure.[19–21] Calculations are converged to an orbital gradient *i.e.* DIIS error of 10^{-7}, unless otherwise stated.

Calculations within the fully spin-restricted, fully spin-unrestricted, as well as spin-restricted open-shell via the constrained unrestricted HF[65,66] formalisms are supported. The orbitals obtained by full diagonal-

ization of the Fock matrix by m block. As described in ref. 1, because the finite element basis set is never ill-conditioned, symmetric orthonormalization is used to construct the molecular orbital basis set, but the basis functions are normalized before the orthonormalization procedure.

Although the present implementation supports the same four grid types discussed in part I for the atomic calculations,[1] a linear grid in $\mu \in [0, \mu_\infty]$ is used for all calculations in the present work, as the (μ, ν, ϕ) coordinate system already yields wave functions that are smooth enough for efficient numerical representation as was discussed in the Introduction. Following the atomic calculations of ref. 1, the calculations in the present work employ 15^{th} order Lobatto elements in the radial expansion, which allow for extremely fast convergence to the radial basis set limit.

4 Results

4.1 HF limit energies

43 first- and second-row molecules from ref. 29, and 27 transition metal molecules from ref. 30 are studied; the molecules and their ROHF limit energies are listed in tables 2 and 3, respectively. All molecules have a wave function with Σ symmetry; that is, the net value for m for the occupied orbitals is zero in each spin channel.

The initial HelFEM calculations on NH, ScF, ScCl, ScS, TiN, CrC, MnC^-, FeC, $CrMn^+$, and VO^- were found to converge to a higher-lying solution. In most cases, it was enough to rectify the occupations of the initial guess, but for ScS the occupations had to be frozen for an additional three iterations for the correct occupations to become stable in the Aufbau solution. After a manual correction to the initial guess symmetry, we were still unable to reproduce the energies reported in ref. 30 for CrC, MnC^-, FeC, and $CrMn^+$, requiring an in-depth study of these systems.

We were unable to identify the proper ground state symmetry of these four molecules with commonly-used Gaussian-basis programs, which lack the possibility to enforce the full linear symmetry of the occupied orbitals. The difficult convergence, especially in the case of MnC^-, is likely caused by a large number of low-lying configurations. Although the symmetries can readily be restricted in HelFEM, the reliable determination of the energy ranking of the various configurations was found to require the use of large numerical basis sets: if an insufficiently large numerical basis set was used, configurations that are well-separated in energy in a fully converged calculation erroneously turned out degenerate.

In order to allow quick exploratory calculations, linear symmetry restrictions were implemented in the Gaussian-basis Erkale program.[22,23] Then, by enumerating all the possible orbital occupations yielding Σ symmetry, while restricting the number of α orbitals in every m channel be at least that of β orbitals, a brute-force search for the true ground state configuration of CrC, MnC^-, FeC, and $CrMn^+$ was conducted in Erkale with the fully uncontracted aug-pc-n basis sets,[67–70] yielding the results in table 4. In contrast to the fully numerical calculations, configuration energy orderings are reproduced correctly by even small Gaussian basis sets, as shown by the data in table 4.

According to the data in table 4, the reference energy given for $CrMn^+$ in ref. 30 is incorrect, as the absolute energy deviates by 2.6 eV from the reference value of ref. 30 even in the fully decontracted quintuple-ζ calculation; a similar deviation was also reproduced with the quintuple-ζ aug-cc-pV5Z correlation consistent basis set.[71–73] For this reason, $CrMn^+$ was excluded from the present study. The Gaussian basis set data also show that the ROHF limit energy given in ref. 30 for MnC^- is not fully converged, as the variational calculation in the Gaussian basis reproduced a lower energy than that of the fully numerical x2dhf calculation of ref. 30.

Next, fixing the orbital occupations of CrC, MnC^-, and FeC to the ground state configuration found with Erkale, it was found that the HelFEM calculations for CrC and MnC^- failed to converge within 50 SCF iterations with the core guess. Further calculations in Erkale showed that the problem was caused by the bad guess, which is especially poor for heavy atoms:[60] the Gaussian basis calculations also failed to converge with the core guess. However, we have recently proposed a simple solution to this problem in ref. 60: a good starting guess is obtained simply by using radially screened nuclear charges, which can be obtained from fully numerical calculations on atoms similar to the ones discussed in part I.[1] The superposition of atomic potentials (SAP) guess described in ref. 60 was implemented in HelFEM, and it was used with an LDA exchange-only potential to form initial guesses for CrC, MnC^-, and FeC, after which

molecule	bond length	energy	molecule	bond length	energy	molecule	bond length	energy
$^1CH^+$	$2.137a_0$	-37.9099112	^3NF	$2.49a_0$	-153.8424212	^3NCl	$3.14a_0$	-513.9070135
$^3CH^-$	$2.20a_0$	-38.2933200	$^1OF^-$	$2.82a_0$	-174.2363416	^1SiO	$2.853a_0$	-363.8553418
^3NH	$1.9614a_0$	-54.9784239	$^1F_2$	$2.668a_0$	-198.7734448	$^3PO^-$	$2.90a_0$	-415.6564658
$^1OH^-$	$1.781a_0$	-75.4188031	$^2F_2^-$	$3.52a_0$	-198.8623615	^3SO	$2.87a_0$	-472.3991048
^1FH	$1.7328a_0$	-100.0708025	$^3SiH^-$	$2.94a_0$	-289.4646301	$^1SF^-$	$3.22a_0$	-497.0283470
$^1C_2$	$2.358a_0$	-75.4065652	$^1SH^-$	$2.551a_0$	-398.1497909	^3PF	$3.015a_0$	-440.2339252
^2CN	1.1718 Å	-92.2251382	^1HCl	$2.44a_0$	-460.1124493	^1ClF	$3.14a_0$	-558.9176263
$^1CN^-$	$2.214a_0$	-92.3489506	^2CP	$3.08a_0$	-378.4746084	^1SiS	1.93 Å	-686.5162842
$^1N_2$	$2.068a_0$	-108.9938256	$^1CP^-$	$3.00a_0$	-378.5615887	$^1P_2$	$3.578a_0$	-681.5002553
$^1NO^+$	$2.007a_0$	-128.9780515	^1CS	$2.89964a_0$	-435.3624203	$^3PS^-$	$3.80a_0$	-738.3397074
$^3NO^{-a}$	$2.36a_0$	-129.2801745	^2SiN	1.575 Å	-343.2970269	$^3S_2$	$3.642a_0$	-795.0915590
^1CO	$2.132a_0$	-112.7909072	$^1SiN^-$	$2.94a_0$	-343.3623656	$^1SCl^-$	$4.06a_0$	-857.1044186
$^3O_2$	$2.270a_0$	-149.6687572	^1NP	$2.8173a_0$	-395.1883954	$^1Cl_2$	$3.86a_0$	-919.0089345
$^1CF^+$	$2.322a_0$	-136.9001348	$^3SN^-$	$3.12a_0$	-451.9876493	$^2Cl_2^-$	$5.00a_0$	-919.0795637
$^3CF^-$	$2.78a_0$	-137.2244562						

Table 2: List of studied systems and restricted HF limit energies from ref. 29. All wave functions have Σ symmetry.
[a]Reference ref. 29 erroneously reports a singlet state for NO^-.

molecule	bond length	energy	molecule	bond length	energy	molecule	bond length	energy
^{1}ScCl	2.229 Å	-1219.335786	^{2}TiN	1.5802 Å	-902.769282	^{1}NiC	1.631 Å	-1544.389546
^{1}ScF	1.787 Å	-859.301233	^{1}TiN$^+$	1.586 Å	-902.526865	^{1}NiSi	2.075 Å	-1795.561185
^{1}ScH	1.775 Å	-760.277980	^{3}VO$^-$	1.615 Å	-1017.767081	^{1}CuH	1.463 Å	-1639.514112
^{2}ScN$^+$	1.738 Å	-813.905803	^{3}CrC	1.63 Å	-1080.868066	^{1}CuF	1.745 Å	-1738.465275
^{1}ScN	1.687 Å	-814.088437	^{1}CrMn$^+$	2.41 Å	-2192.467304^a	^{1}CuCl	2.051 Å	-2098.548160
^{1}ScO$^+$	1.651 Å	-834.441524	^{3}MnC$^-$	1.615 Å	-1187.323508^a	^{1}Cu$_2$	2.22 Å	-3277.941606
^{2}ScO	1.6682 Å	-834.674512	^{3}FeC	1.670 Å	-1299.926272	^{1}CuLi	2.26 Å	-1646.409856
^{1}ScS$^-$	2.188 Å	-1157.375086	^{1}CoC$^-$	1.564 Å	-1418.878845	^{2}ZnH	1.595 Å	-1778.377824
^{2}ScS	2.135 Å	-1157.338534	^{3}CoO$^-$	1.616 Å	-1456.143757	^{2}ZnF	1.768 Å	-1877.344833

Table 3: List of studied systems and restricted HF limit energies from ref. 30. All wave functions have Σ symmetry. ^{a}The reference values for CrMn$^+$ and MnC$^-$ are incorrect, see main text.

molecule	un-aug-pc-1		un-aug-pc-2		un-aug-pc-3		un-aug-pc-4	
	Δ	$E - E_{\mathrm{ref}}$	Δ	$E - E_{\mathrm{ref}}$	Δ	$E - E_{\mathrm{ref}}$	Δ	$E - E_{\mathrm{ref}}$
CrC	4.446	2.480	4.402	0.159	4.393	0.016	4.389	0.003
MnC^-	3.179	2.666	3.118	0.156	3.109	0.001	3.103	-0.012
FeC	1.677	2.787	1.542	0.169	1.514	0.015	1.509	0.002
$CrMn^+$	0.843	6.923	0.891	2.931	0.897	2.681	0.899	2.647

Table 4: Energy difference Δ between the lowest configuration and second lowest configuration for CrC, MnC^-, FeC, and $CrMn^+$ found in the brute-force search with the fully uncontracted aug-pc-n basis sets (un-aug-pc-n), as well as the difference of the ground-state energy from the Gaussian calculation to the numerical reference value from ref. 30, $E - E_{\mathrm{ref}}$. All values are in eV.

the fully numerical calculations on these molecules converged without problems. For MnC^- and $CrMn^+$ at the studied geometries, we find the fully numerical energies -1187.3240938 and -2192.3703627, respectively. These are in good agreement with the values computed with ERKALE in the fully decontracted aug-pc-4 basis set: -1187.3239603 and -2192.3700339, respectively. Our fully numerical reference value for MnC^- is 586 μE_h lower than the one given in ref. 30, whereas the 2.64 eV discrepancy for $CrMn^+$ suggests that the ROHF limit value of ref. 30 does not correspond to the reported charge, spin state, and/or geometry.

Excluding $CrMn^+$ and MnC^- for which the literature values are incorrect, we obtain the convergence behavior shown in figures 1 and 2 for the 43 main group and 25 transition metal molecules, respectively. Both figures present results for $r_\infty = 20a_0$, $r_\infty = 40a_0$, and $r_\infty = 60a_0$. It is clear from these results that the chosen proxy is remarkably successful in capturing the essential degrees of freedom in the basis set, as the error in the self-consistent energy is seen to follow that in the proxy within an order of magnitude until $\epsilon = 10^{-5}$, when the error starts to saturate. The error levels off because of the finite accuracy of the reference data: the HF limit energies for the main group and transition metal molecules have been given with 7 and 6 decimals in refs. 29 and 30, respectively, which were also repeated in tables 2 and 3.

As was discussed in the first part of this series dealing with atomic calculations,[1] the value for the practical infinity $r_\infty = 20a_0$ is too small, yielding significant errors especially in anionic systems, as can be seen from the outliers in figures 1 and 2 that do not exist in the $r_\infty = 40a_0$ and $r_\infty = 60a_0$ plots. Based on these results and those obtained for atoms in part I,[1] we tentatively conclude that $r_\infty = 40a_0$ should be sufficient for applications of the present method. However, the convergence with respect to r_∞ should be always checked, as loosely bound anions be extremely diffuse – especially in DFT calculations – as was discussed in the first part of the series.[1]

Despite the spread in the results and the finite accuracy of the reference data, it is clear that choosing a basis with an estimated accuracy of $\epsilon = 10^{-10}$ should yield energies that are converged beyond microhartree accuracy. Indeed, in some cases HELFEM reproduces variational energies that are considerably *lower* than the previous reference values. For instance, the best energy reported for Cl_2^- in ref. 29 is -919.0795637, whereas the $\epsilon = 10^{-10}$ basis set for $r_\infty = 40a_0$ in HELFEM yields the value -919.0795645 that is $0.8\mu E_h$ lower.

This is all the more striking, as the basis set used for the HELFEM calculation is considerably smaller than the one that was used to reproduce the value in ref. 29. The more accurate HELFEM value was obtained with $r_\infty = 40a_0$, yielding 98 basis functions in μ. In contrast, the X2DHF calculation of ref. 29 needed $r_\infty = 400a_0$ and 535 points in the radial μ grid to converge the energy. As has been discussed above, X2DHF uses an asymptotic expansion to calculate the Coulomb and exchange potentials, requiring r_∞ to be much larger than what it would be based on the density alone, as in HELFEM. However, since the size of the μ grid scales logarithmically in r_∞ (equation (13)), this is not a huge problem: $\mu_\infty \approx 5.78$ in the X2DHF calculation, compared to $\mu_\infty \approx 3.46$ in the HELFEM calculation, meaning that a 67% larger μ grid would naïvely suffice in the X2DHF calculation.

Instead, the main reason HELFEM yields better accuracy despite needing over five times fewer radial functions is that it uses high-order elements that afford extremely fast convergence to the radial basis set limit, as was found in ref. 1. In addition to a more compact radial expansion by over a factor of five, also the angular expansion is much more compact in HELFEM: compared to the 295 points in ν used for Cl_2^- in ref. 29, the more accurate $r_\infty = 40a_0$, $\epsilon = 10^{-10}$ HELFEM calculation in the present work employed only

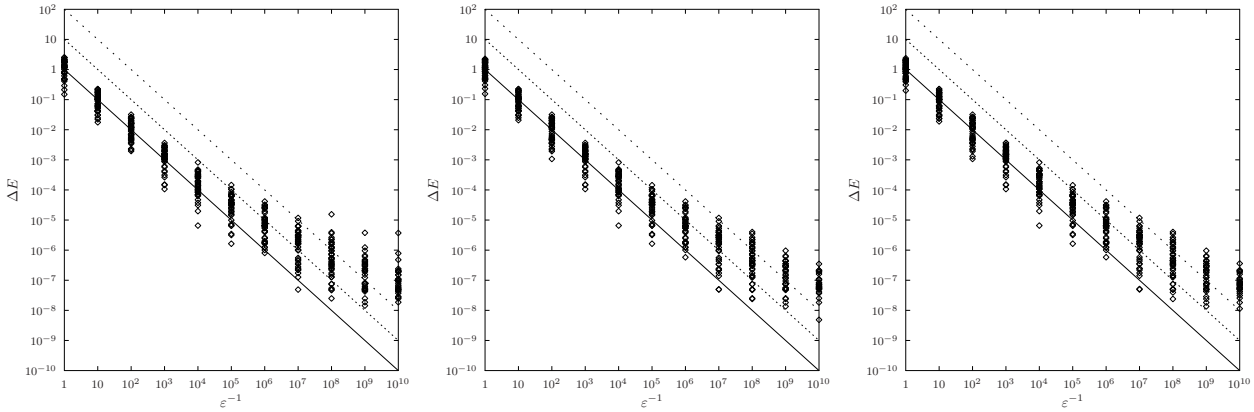

(a) $r_\infty = 20a_0$ (b) $r_\infty = 40a_0$ (c) $r_\infty = 60a_0$

Figure 1: Convergence of the restricted HF energy for 43 first- and second-row molecules, compared to literature values from ref. 29 given in table 2. Note logarithmic scale. The ideal behavior $\Delta E = \epsilon$ is represented by the solid line, with the dotted and loosely dotted lines illustrating behavior corresponding to $\Delta E = 10\epsilon$ and $\Delta E = 100\epsilon$, correspondingly.

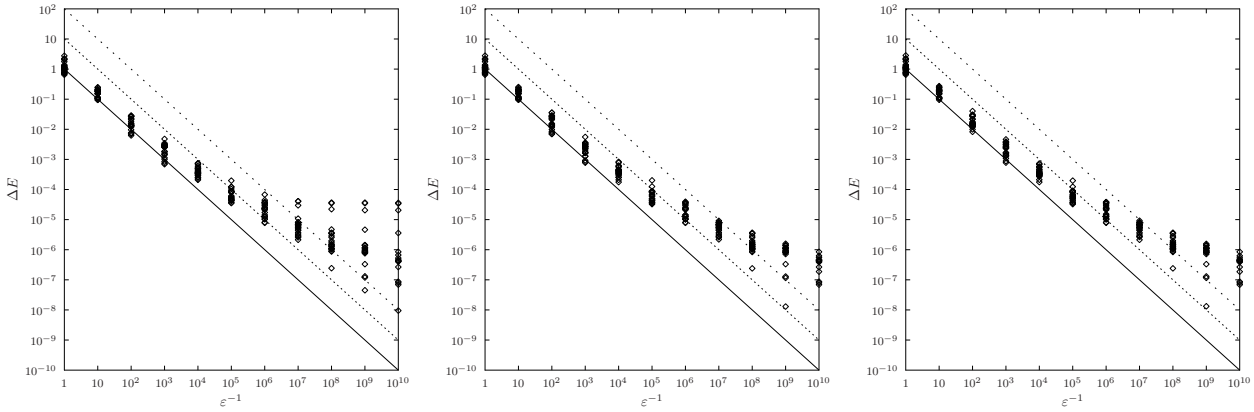

(a) $r_\infty = 20a_0$ (b) $r_\infty = 40a_0$ (c) $r_\infty = 60a_0$

Figure 2: Convergence of the restricted HF energy for 25 transition metal molecules, compared to literature values from ref. 30 given in table 3. MnC^- and $CrMn^+$ have been excluded, as the reference values are incorrect. Note logarithmic scale. The notation is the same as in figure 1.

39 σ functions ($l_\sigma = 38$) and 29 π_{+1} and π_{-1} functions ($l_\pi = 29$), indicating a further reduction by an order of magnitude in the size of the basis set.

Tables 5 and 6 show comparisons of the basis sets to obtain results with a microhartree-level accuracy employed in refs. 29 and 30, respectively, to the $r_\infty = 40a_0$, $\epsilon = 10^{-10}$ basis sets used in the present work. These results are fully in line with the discussion above for the case of Cl_2^-, showing that the combination of high-order finite elements and the partial wave expansion in HelFEM allow for basis sets that are more compact by orders of magnitude compared to the approach used in the x2dhf program.

Having shown that the proxy basis sets are capable of reproducing energies at the ROHF limit, for reference, updated ROHF reference values, computed in the $r_\infty = 60a_0$, $\epsilon = 10^{-10}$ basis set for the 70 diatomic molecules of refs. 29 and 30 are shown in table 7. In most cases, the change is but a different round-off of the last decimal; however, the changes to the ROHF limit energy of $^3SiH^-$ and $^2Cl_2^-$ as well as the aforementioned $^1CrMn^+$ and $^3MnC^-$ are more noticeable. In addition, we have repeated the calculations with unrestricted HF for the molecules for which non-singlet states were specified; these results are shown in table 8. The energy lowerings from ROHF range from 0.44 mE_h for ScO to 241.6 mE_h for FeC; these results were likewise obtained with the $r_\infty = 60a_0$, $\epsilon = 10^{-10}$ basis set.

4.2 Electric properties of BH and N_2

Next, to demonstrate further capabilities of the program, we run finite field HF calculations on the BH ($R = 2.3289a_0$) and N_2 ($R = 2.068a_0$) molecules and compare the results with literature values computed at the basis set limit from ref. 74, complemented with unpublished data from the same work.[75] Five radial elements are used with $r_\infty = 40a_0$ with the angular basis $l_\sigma = 20$, $l_\pi = 15$ for both molecules; this yields the values in table 9. For comparison, the basis with $\epsilon = 10^{-10}$ would have three radial elements and $l_\sigma = 17$, $l_\pi = 11$ for N_2 and $l_\sigma = 15$, $l_\pi = 11$ for BH at the used geometries.

For BH, the energies in table 9 match to nanohartree-level accuracy. The dipole and quadrupole moments only disagree in the fifth and sixth decimals, respectively, again indicating an excellent level of agreement. What makes this remarkable is that ref. 74 employed 349 points in ν and 643 points in μ with $r_\infty = 200a_0$, whereas the calculations in the present work employ but 21 σ waves and 15 π waves, and 70 shape functions in μ with $r_\infty = 40a_0$. That is, we obtain excellent accuracy despite having used *over two orders of magnitude* fewer parameters (a factor of over 150) for the wave function, in line with the results that were obtained above in section 4.1 for the field-free case.

For N_2, the energies again agree to nanohartree-level accuracy, whereas differences in the dipole and quadrupole moments are now seen already at the fourth and fifth decimals, respectively. Ref. 74 employed an even larger grid for N_2 than for BH: 841 points in μ and 445 points in ν, whereas the present calculations only use the same small number of parameters as for BH. Again, a reduction of over two orders of magnitude is achieved, underlining the power of the present approach.

Employing the data in table 9, we obtain the polarizabilities 22.561246 and 22.560787 for BH and 14.950727 and 14.949617 for N_2, employing the two-point

$$f'(x) \approx \frac{f(x+h) - f(x-h)}{2h} \tag{92}$$

and four-point

$$f'(x) \approx \frac{-f(x+2h) + 8f(x+h) - 8f(x-h) + f(x-2h)}{12h} \tag{93}$$

stencils, respectively. These results compare favorably with the literature values[74] 22.560640 for BH and 14.9512154 for N_2: the discrepancy for the four-point value for BH is at the sixth significant number – well within the estimated numerical error bounds – whereas for N_2 the discrepancy is already seen at the fifth significant number, still yielding good agreement.

4.3 Atomization energy of N_2

As a final demonstration, we study the convergence of the atomization energy

$$\Delta E = \sum_{\text{atoms } i} E_i^{\text{atom}} - E^{\text{molecule}} > 0 \tag{94}$$

	X2DHF			HELFEM				X2DHF			HELFEM				X2DHF			HELFEM		
molecule	r_∞	n_μ	n_ν	n_μ	l_σ	l_π	molecule	r_∞	n_μ	n_ν	n_μ	l_σ	l_π	molecule	r_∞	n_μ	n_ν	n_μ	l_σ	l_π
$^1CH^+$	30	193	163	42	15	11	^3NF	200	319	175	70	19	15	^3NCl	300	409	217	98	29	23
$^3CH^-$	40	229	169	42	15	11	$^1OF^-$	200	313	175	70	21	17	^1SiO	200	313	175	70	25	19
^3NH	40	235	169	42	15	13	$^1F_2$	300	337	175	70	21	15	$^3PO^-$	300	415	217	70	27	21
$^1OH^-$	40	241	169	42	15	13	$^2F_2^-$	400	421	217	70	23	17	^3SO	350	421	217	98	27	21
^1FH	30	193	169	70	17	13	$^3SiH^-$	200	307	175	70	27	19	$^1SF^-$	300	403	217	98	29	23
$^1C_2$	40	223	169	42	17	11	$^1SH^-$	300	421	217	70	27	21	^3PF	300	409	217	70	27	21
^2CN	40	229	169	42	17	13	^1HCl	200	319	175	70	27	21	^1ClF	350	415	217	98	29	23
$^1CN^-$	40	229	169	42	17	13	^2CP	200	307	175	70	27	21	^1SiS	300	475	259	98	31	23
$^1N_2$	40	229	169	42	17	11	$^1CP^-$	300	409	217	70	27	21	$^1P_2$	400	499	259	98	31	23
$^1NO^+$	40	235	169	42	17	13	^1CS	200	307	175	70	27	21	$^3PS^-$	350	481	259	98	31	23
$^3NO^-$ [a]	200	319	175	70	19	15	^2SiN	200	307	175	70	27	21	$^3S_2$	350	481	259	98	31	23
^1CO	40	229	169	70	17	13	$^1SiN^-$	200	307	175	70	27	21	$^1SCl^-$	400	487	259	98	33	25
$^3O_2$	200	325	175	70	19	13	^1NP	200	313	175	70	27	21	$^1Cl_2$	400	493	259	98	37	29
$^1CF^+$	40	223	169	70	19	15	$^3SN^-$	350	415	217	98	29	21	$^2Cl_2^-$	400	505	277	98	37	29
$^3CF^-$	200	313	175	70	21	15														

Table 5: Comparison of the smallest numerical basis sets (r_∞, n_μ, n_ν) yielding at least six correct decimals by rounding in X2DHF calculations on main-group molecules, taken from ref. 29, versus the $\epsilon = 10^{-10}$ proxy basis sets reproduced by HELFEM with $r_\infty = 40$ with n_μ radial functions and l_σ and l_π partial waves, which reproduce the reference values of ref. 29 beyond microhartree accuracy (present work). [a]Reference ref. 29 erroneously reports a singlet state for NO^-.

	X2DHF			HELFEM					X2DHF			HELFEM					X2DHF			HELFEM			
molecule	r_∞	n_μ	n_ν	n_μ	l_σ	l_π	l_δ	molecule	r_∞	n_μ	n_ν	n_μ	l_σ	l_π	l_δ	molecule	r_∞	n_μ	n_ν	n_μ	l_σ	l_π	l_δ
^{1}ScCl	350	541	295	98	38	28	24	^{2}TiN	350	577	295	98	34	26	22	^{1}NiC	350	571	295	126	38	28	24
^{1}ScF	250	409	229	98	34	26	22	^{1}TiN$^+$	350	571	295	98	34	26	22	^{1}NiSi	400	619	325	126	42	32	26
^{1}ScH	350	565	295	98	34	26	22	^{3}VO$^-$	350	571	295	98	34	26	22	^{1}CuH	350	583	295	98	36	28	24
^{2}ScN$^+$	350	565	295	98	34	26	22	^{3}CrC	350	571	295	98	36	26	22	^{1}CuF	400	637	325	126	40	30	26
^{1}ScN	250	415	229	98	34	26	22	^{1}CrMn$^+$ [a]	400	601	325	126	44	32	28	^{1}CuCl	350	547	295	126	44	32	28
^{1}ScO$^+$	350	571	295	98	34	24	22	^{3}MnC$^-$ [a]	350	571	295	98	36	26	22	^{1}Cu$_2$	425	685	361	126	46	34	28
^{2}ScO	250	415	229	98	34	26	22	^{3}FeC	350	571	295	98	38	28	24	^{1}CuLi	400	607	325	126	46	34	28
^{1}ScS$^-$	350	541	295	98	38	28	24	^{1}CoC$^-$	350	577	295	98	36	28	24	^{2}ZnH	350	571	295	126	40	30	24
^{2}ScS	350	547	295	98	38	28	24	^{3}CoO$^-$	400	643	325	98	38	28	24	^{2}ZnF	350	565	295	126	42	30	26

Table 6: Comparison of the smallest numerical basis sets (r_∞, n_μ, n_ν) yielding the energy converged to microhartrees, taken from ref. 30, versus the $\epsilon = 10^{-10}$ proxy basis sets reproduced by HELFEM with $r_\infty = 40$ with n_μ radial functions and l_σ and l_π partial waves, which reproduce the reference values beyond microhartree accuracy (present work). [a]The reference values reported in ref. 30 are incorrect for $CrMn^+$ and MnC^-, see main text.

molecule	energy	molecule	energy	molecule	energy
^{3}NH	-54.978423**8**	^{2}CP	-378.474608**3**	^{3}PS$^-$	-738.339707**0**
^{1}OH$^-$	-75.418803**0**	^{1}CP$^-$	-378.561588**6**	^{3}S$_2$	-795.091559**1**
^{1}CN$^-$	-92.348950**5**	^{1}CS	-435.362420**1**	^{1}SCl$^-$	-857.104418**4**
^{1}NO$^+$	-128.978051**4**	^{2}SiN	-343.297026**8**	^{1}Cl$_2$	-919.008934**8**
^{3}NO$^-$	-129.280174**6**	^{1}SiN$^-$	-343.362365**5**	^{2}Cl$_2^-$	-919.079564**6**
^{3}O$_2$	-149.668757**3**	^{1}NP	-395.188395**3**	^{1}ScCl	-1219.335785**4**
^{3}CF$^-$	-137.224456**1**	^{3}SN$^-$	-451.987649**2**	^{1}ScO$^+$	-834.441532**2**
^{3}NF	-153.842421**1**	^{3}NCl	-513.907013**4**	^{1}CrMn$^+$	-2192.**370362**7
^{1}OF$^-$	-174.236341**7**	^{1}SiO	-363.855341**6**	^{3}MnC$^-$	-1187.32**4093**4
^{1}F$_2$	-198.773444**9**	^{1}ClF	-558.917626**4**	^{3}CoO$^-$	-1456.143756**5**
^{3}SiH$^-$	-289.4646**29**9	^{1}SiS	-686.516284**0**	^{1}Cu$_2$	-3277.941606**7**
^{1}SH$^-$	-398.149790**8**				

Table 7: ROHF limit values updated from tables 2 and 3 using the corresponding $r_\infty = 60a_0$, $\epsilon = 10^{-10}$ basis set, with changed digits shown in bold.

molecule	energy	molecule	energy	molecule	energy
CH$^-$	-38.2994602	SiN	-343.3130427	ScO	-834.6749525
NH	-54.9863336	SN$^-$	-452.0046200	ScS	-1157.3394254
CN	-92.2425169	NCl	-513.9187494	TiN	-902.7833285
NO$^-$	-129.2959898	PO$^-$	-415.6654029	VO$^-$	-1017.7882900
O$_2$	-149.6922860	SO	-472.4170546	CrC	-1081.0323244
CF$^-$	-137.2322589	PF	-440.2409912	MnC$^-$	-1187.5638036
NF	-153.8527981	PS$^-$	-738.3489562	FeC	-1300.1679109
F$_2^-$	-198.8783311	S$_2$	-795.1075610	CoO$^-$	-1456.2267835
SiH$^-$	-289.4704308	Cl$_2^-$	-919.0880177	ZnH	-1778.3801627
CP	-378.4754390	ScN$^+$	-813.9079564	ZnF	-1877.3457934

Table 8: Unrestricted HF energies for the main group and transition metal systems obtained with the corresponding $r_\infty = 60a_0$, $\epsilon = 10^{-10}$ basis set, using the geometries and spin states given in tables 2 and 3.

BH, $R = 2.3289a_0$

	Present work			Literature value		
E_z	Energy[a]	Dipole	Quadrupole	Energy[b]	Dipole[b]	Quadrupole[c]
-8×10^{-4}	-25.132024018	6.669105 (-1)	-3.968475 (0)	-25.132024018	6.669096 (-1)	-3.968472 (0)
-4×10^{-4}	-25.131829783	6.759386 (-1)	-3.985054 (0)	-25.131829783	6.759377 (-1)	-3.985051 (0)
0	-25.131639159	6.849639 (-1)	-4.001849 (0)	-25.131639159	6.849630 (-1)	-4.001846 (0)
4×10^{-4}	-25.131452145	6.939876 (-1)	-4.018863 (0)	-25.131452145	6.939866 (-1)	-4.018861 (0)
8×10^{-4}	-25.131268739	7.030107 (-1)	-4.036098 (0)	-25.131268740	7.030097 (-1)	-4.036096 (0)

N_2, $R = 2.068a_0$

	Present work			Literature value		
E_z[d]	Energy	Dipole	Quadrupole	Energy[b]	Dipole[b]	Quadrupole[b]
-1.6×10^{-3}	-108.993844772	-2.392544 (-2)	-9.401255 (-1)	-108.993844772	-2.392249 (-2)	-9.401254 (-1)
-0.8×10^{-3}	-108.993830419	-1.196071 (-2)	-9.399594 (-1)	-108.993830419	-1.196104 (-2)	-9.399567 (-1)
0	-108.993825634	-9.782586 (-13)	-9.399016 (-1)	-108.993825635	-3.463896 (-14)	-9.399005 (-1)
0.8×10^{-3}	-108.993830419	1.196071 (-2)	-9.399594 (-1)	-108.993830419	1.196104 (-2)	-9.399567 (-1)
1.6×10^{-3}	-108.993844772	2.392544 (-2)	-9.401255 (-1)	-108.993844772	2.392249 (-2)	-9.401254 (-1)

Table 9: Electric properties of BH and N_2 in a finite field, compared to literature values. The values in the parentheses indicate magnitude, $A(n) = A \times 10^n$.

[a]The energy for HelFEM is offset to match that of ref. 74, due to a difference in the definition of the zero-point of the nuclear dipole – electric field interaction.

[b]Literature values are from ref. 74 with a truncated number of decimals.

[c]The values for the quadrupole moment of BH with respect to the center of the molecule for were obtained from ref. 75.

[d]Note that the values for the field reported in Table V of ref. 74 correspond in fact to the F_z values given above instead of $\pm 0.6 \times 10^{-3}$ and $\pm 1.2 \times 10^{-3}$.[75]

of N_2 at the geometry given in table 9 with HF, and the LDA,[76–78] PBE,[79,80] PBE0,[81,82] BP86,[83,84] BLYP,[83,85] B3LYP,[86,87] revTPSS,[88,89] revTPSSh,[88–90] MS2,[88,91] and MS2h[88,91] functionals. Although atomic energies can be computed most efficiently with the atomic program presented in part I,[1] the atomization energy can be extracted more accurately by running the atomic calculations in the same basis set as the diatomic molecule, achieved by setting the other nuclear charge to 0, in analogy to the Boys–Bernardi counterpoise method of LCAO calculations.[92] Such a procedure results in significant error cancellation: the largest error in the total energy for both the individual atoms and the molecule arises from an incomplete description in ν of the core region, which requires many partial waves to converge fully. By computing the atomic energies in the same basis set, the errors arising from the core region cancel out almost perfectly.

The results with this method are shown in table 10, highlighting excellent, monotonic convergence for all methods. Note that unlike figures 1 and 2, table 10 does not contain values for arbitrary values of ϵ, as the estimated error in the proxy energy may decrease by several orders of magnitude per step: for example, the $\epsilon = 10^{-3}$ basis is the same as the $\epsilon = 10^{-4}$ basis. The atomization energy evaluated with the fully numerical approach appears to be converged to 0.1 meV accuracy with all methods except MS2 and MS2h, for which convergence is slightly poorer; this can likely be attributed to the MS2 exchange functional being numerically less well-conditioned than the other functionals in the present study.

For comparison, table 11 shows the corresponding calculations performed with Erkale[22,23] in the pcseg-n and aug-pcseg-n basis sets.[67,68,93] A (350,974) DFT quadrature grid and the Boys–Bernardi counterpoise correction[92] were employed to ensure benchmark quality results. The largest differences between the HelFEM and Erkale results with the best basis sets, $\epsilon = 10^{-10}$ and aug-pcseg-4, respectively, are seen for the MS2 (43.7 meV) and MS2h (40.2 meV) functionals, again likely caused by the numerical properties of the MS2 exchange functional. The revTPSS and revTPSSh values disagree by 12.6 meV and 10.6 meV, respectively. The disagreements for the other functionals are in the range of 2–6 meV. Although the number of basis functions in the Gaussian basis calculations is much smaller than in the partial wave approach, convergence with the Gaussian basis sets is not always monotonic, unlike what was observed in table 10 for the partial wave method.

5 Summary

We have presented a new finite element implementation of the partial wave approach for diatomic molecules in the HelFEM program[13] for electronic structure calculations with Hartree–Fock (HF) or density functional theory (DFT). HelFEM supports hundreds of functionals within the local spin density approximation (LDA), generalized gradient approximation (GGA), as well as meta-GGA approximation – including hybrid functionals – via an interface to the Libxc library.[14] The orbitals can be fully spin-restricted, spin-restricted open-shell, or fully spin-unrestricted in calculations.

We have proposed a novel way to cost-efficiently choose the fully numerical basis set for calculations on diatomic molecules by optimizing the completeness of the basis set to reproduce the lowest eigenstates of the core Hamiltonian. By applying the procedure to calculations on 70 diatomic molecules with published restricted open-shell HF limit energies from the literature, we showed that the approach is able to easily and controllably reproduce energies at a sub-microhartree level accuracy, requiring a significantly smaller number of parameters for the wave function than what was originally needed to generate the literature values. Further applications of the program to the electric properties of BH and N_2 under finite field also showed excellent agreement with previously published values, even though over two orders of magnitude fewer parameters were used for the wave function in the present work. The application of the program to the atomization energy of N_2 with HF and local spin density (LDA), generalized gradient approximation (GGA), and meta-GGA functionals and comparison to Gaussian basis set calculations further underlined the robustness of the present approach. The extension of the present work to finite magnetic fields has been discussed in ref. 32.

6 Discussion

Although many systems are already tractable with the present version of HelFEM, it is evident that as a novel program, many further optimizations are possible. This is especially clear from McCullough's

basis	n_{bf}	HF	LDA	PBE	PBE0	BP86	BLYP	B3LYP	revTPSS	revTPSSh	MS2	MS2h
10^{-0}	190	9.5597	16.3779	15.0682	14.2955	15.1409	15.0568	14.6154	14.4547	14.1898	14.4645	14.2433
10^{-1}	242	5.2812	11.9074	10.8646	10.0738	10.8872	10.7276	10.2628	10.2409	9.9694	10.4266	10.1814
10^{-2}	830	5.1822	11.8001	10.7499	9.9632	10.7757	10.6138	10.1523	10.1173	9.8482	10.3602	10.1108
10^{-4}	1078	5.0307	11.6257	10.5800	9.7979	10.6053	10.4405	9.9826	9.9589	9.6903	10.1846	9.9375
10^{-7}	1326	5.0268	11.6216	10.5751	9.7932	10.6004	10.4357	9.9780	9.9533	9.6849	10.1760	9.9297
10^{-9}	1574	5.0267	11.6215	10.5751	9.7932	10.6003	10.4356	9.9779	9.9532	9.6849	10.1759	9.9297
10^{-10}	1658	5.0267	11.6215	10.5751	9.7932	10.6003	10.4356	9.9779	9.9531	9.6848	10.1752	9.9291

Table 10: Atomization energy of N_2 in eV with HF and the LDA, PBE, PBE0, BP86, BLYP, B3LYP, revTPSS, revTPSSh, MS2, and MS2h functionals, employing the partial wave expansion with the adaptive grid method.

basis	n_{bf}	HF	LDA	PBE	PBE0	BP86	BLYP	B3LYP	revTPSS	revTPSSh	MS2	MS2h
pcseg-0	18	2.4926	9.9488	8.9278	7.8865	8.9383	8.8661	8.1961	8.1253	7.7757	8.2910	7.9759
pcseg-1	28	4.7316	11.2740	10.2694	9.4830	10.2788	10.0954	9.6412	9.6875	9.4147	9.8871	9.6381
pcseg-2	60	4.9930	11.5768	10.5323	9.7514	10.5618	10.3910	9.9342	9.9190	9.6509	10.1092	9.8655
pcseg-3	120	5.0343	11.6096	10.5572	9.7828	10.5876	10.4181	9.9670	9.9400	9.6744	10.1243	9.8831
pcseg-4	202	5.0303	11.6179	10.5673	9.7887	10.5944	10.4289	9.9743	9.9387	9.6727	10.1303	9.8878
aug-pcseg-0	26	2.3501	9.6348	8.5963	7.6248	8.6306	8.5292	7.9169	7.8346	7.5088	8.0288	7.7309
aug-pcseg-1	46	4.7695	11.3205	10.2978	9.5209	10.3128	10.1309	9.6840	9.7068	9.4388	9.9076	9.6624
aug-pcseg-2	92	5.0070	11.5865	10.5408	9.7616	10.5688	10.3990	9.9437	9.9264	9.6592	10.1171	9.8742
aug-pcseg-3	170	5.0364	11.6177	10.5681	9.7898	10.5949	10.4290	9.9745	9.9475	9.6809	10.1316	9.8895
aug-pcseg-4	274	5.0306	11.6194	10.5690	9.7897	10.5959	10.4308	9.9754	9.9405	9.6742	10.1315	9.8889

Table 11: Atomization energy of N_2 in eV with HF and the LDA, PBE, PBE0, BP86, BLYP, B3LYP, revTPSS, revTPSSh, MS2, and MS2h, employing (aug-)pcseg-n basis sets.

paper from over 30 years ago that reported a spin-restricted single-reference calculation on the $^2\Pi$ state of KO at $4.40a_0$ bond length with $l_{\max} = 29$, with the converged final energy -674.014150 E_h;[39] we have repeated the calculation with the adaptive basis at an estimated 10^{-10} accuracy, yielding $l_\sigma = 37$ and $l_\pi = 27$ with seven 15-node Lobatto elements, yielding the final energy -674.014903429 E_h. As such large calculations were possible already in the mid-1980s, the feasible system size limit with present-day computers and algorithms should be much larger. The venerable X2DHF program might also yield insights into possible further optimizations.

At present, alike the atomic program presented in part I of the series,[1] all matrices in the diatomic program are stored naïvely as dense matrices with the rank $N_{\text{ang}} \times N_{\text{rad}}$, where N_{ang} and N_{rad} are the number of angular and radial basis functions, as this is easier to implement and develop upon than a more specialized storage scheme. However, as was stated by equation (23), the orbitals block by the m quantum number, and so the orbital gradient is also diagonal in m, unless symmetries are broken. This means that the self-consistent field (SCF) problem could in principle be solved using *e.g.* DIIS by only building the (m, m) blocks of the (Kohn–Sham–)Fock matrix, which would mean a savings of a factor of roughly $2m_{\max} + 1$ in the size of the matrix.

However, evaluations of the total energy require also the off-diagonal (m, m') blocks. As the DIIS method only works when the orbitals are sufficiently close to convergence, more robust methods are required for the initial steps of the SCF procedure, before switching over to the DIIS algorithm. But, as the more robust algorithms such as the presently used ADIIS[21] algorithm typically require evaluations of the total energy, the potential savings of not computing the (m, m') blocks for DIIS would be small: the bulk of SCF iterations are typically spent on getting the orbitals close to convergence, after which DIIS converges within a few iterations. The m factor is also quite small even for φ orbitals, for which the saving would be only a factor of 7.

Funding information

This work has been supported by the Academy of Finland through project number 311149.

Acknowledgments

I thank Barry Schneider for invaluable help with Legendre functions, and Dage Sundholm and Jacek Kobus for discussions. I also thank Dage Sundholm, Barry Schneider, Jacek Kobus, and Pekka Pyykkö for comments on the manuscript, as well as Frank Jensen and Jacek Kobus for help in reproducing literature results. Computational resources provided by CSC – It Center for Science Ltd (Espoo, Finland) and the Finnish Grid and Cloud Infrastructure (persistent identifier urn:nbn:fi:research-infras-2016072533) are gratefully acknowledged.

References

[1] S. Lehtola, arXiv p. 1810.11651 (2018), 1810.11651, URL http://arxiv.org/abs/1810.11651.

[2] S. Lehtola, arXiv p. 1902.01431 (2019), 1902.01431, URL http://arxiv.org/abs/1902.01431.

[3] E. A. McCullough, Chem. Phys. Lett. **24**, 55 (1974), ISSN 00092614, URL http://linkinghub.elsevier.com/retrieve/pii/0009261474802125.

[4] E. A. McCullough, J. Chem. Phys. **62**, 3991 (1975), ISSN 0021-9606, URL http://aip.scitation.org/doi/10.1063/1.430322.

[5] D. Heinemann, B. Fricke, and D. Kolb, Chem. Phys. Lett. **145**, 125 (1988), ISSN 00092614, URL http://linkinghub.elsevier.com/retrieve/pii/0009261488801635.

[6] D. Sundholm, J. Olsen, P.-Å. Malmqvist, and B. O. Roos, in *Numer. Determ. Electron. Struct. Atoms, Diatomic Polyat. Mol.* (Springer Netherlands, Dordrecht, 1989), pp. 329–334, URL http://www.springerlink.com/index/10.1007/978-94-009-2329-4_25.

[7] J. Kobus, L. Laaksonen, and D. Sundholm, Comput. Phys. Commun. **98**, 346 (1996), ISSN 00104655, URL http://linkinghub.elsevier.com/retrieve/pii/0010465596000987.

[8] J. Kobus, Comput. Phys. Commun. **184**, 799 (2013), ISSN 00104655, URL http://dx.doi.org/10.1016/j.cpc.2012.09.033http://linkinghub.elsevier.com/retrieve/pii/S0010465512003311.

[9] K. Rüdenberg, J. Chem. Phys. **19**, 1459 (1951), ISSN 0021-9606, URL http://aip.scitation.org/doi/10.1063/1.1748100http://aip.scitation.org/doi/10.1063/1.1748101.

[10] A. N. Artemyev, E. V. Ludeña, V. V. Karasiev, and A. J. Hernández, J. Comput. Chem. **25**, 368 (2004), ISSN 01928651, URL http://doi.wiley.com/10.1002/jcc.10390.

[11] P. Hohenberg and W. Kohn, Phys. Rev. **136**, B864 (1964), ISSN 0031-899X, URL http://link.aps.org/doi/10.1103/PhysRev.136.B864.

[12] W. Kohn and L. J. Sham, Phys. Rev. **140**, A1133 (1965), ISSN 0031-899X, URL http://link.aps.org/doi/10.1103/PhysRev.140.A1133.

[13] S. Lehtola, *HelFEM – Finite element methods for electronic structure calculations on small systems* (2018), URL http://github.com/susilehtola/HelFEM.

[14] S. Lehtola, C. Steigemann, M. J. Oliveira, and M. A. Marques, SoftwareX **7**, 1 (2018), ISSN 23527110, URL http://linkinghub.elsevier.com/retrieve/pii/S2352711017300602https://linkinghub.elsevier.com/retrieve/pii/S2352711017300602.

[15] D. Langreth and J. Perdew, Phys. Rev. B **21**, 5469 (1980), ISSN 0163-1829, URL http://link.aps.org/doi/10.1103/PhysRevB.21.5469.

[16] J. Perdew, S. Kurth, A. Zupan, and P. Blaha, Phys. Rev. Lett. **82**, 2544 (1999), ISSN 0031-9007, URL http://link.aps.org/doi/10.1103/PhysRevLett.82.5179http://link.aps.org/doi/10.1103/PhysRevLett.82.2544.

[17] D. Heinemann, A. Rosén, and B. Fricke, Chem. Phys. Lett. **166**, 627 (1990), ISSN 00092614, URL http://linkinghub.elsevier.com/retrieve/pii/000926149087162K.

[18] D. Heinemann and A. Rosén, Theor. Chim. Acta **85**, 249 (1993), ISSN 0040-5744, URL http://link.springer.com/10.1007/BF01129114.

[19] P. Pulay, Chem. Phys. Lett. **73**, 393 (1980), ISSN 00092614, URL http://linkinghub.elsevier.com/retrieve/pii/0009261480803964.

[20] P. Pulay, J. Comput. Chem. **3**, 556 (1982), ISSN 0192-8651, URL http://doi.wiley.com/10.1002/jcc.540030413.

[21] X. Hu and W. Yang, J. Chem. Phys. **132**, 054109 (2010), ISSN 1089-7690, URL http://www.pubmedcentral.nih.gov/articlerender.fcgi?artid=2830258&tool=pmcentrez&rendertype=abstract.

[22] S. Lehtola, *ERKALE – HF/DFT from Hel* (2018), URL https://github.com/susilehtola/erkale.

[23] J. Lehtola, M. Hakala, A. Sakko, and K. Hämäläinen, J. Comput. Chem. **33**, 1572 (2012), ISSN 01928651, URL http://doi.wiley.com/10.1002/jcc.22987.

[24] J. Hinze, J. Chem. Phys. **59**, 6424 (1973), ISSN 0021-9606, URL http://scitation.aip.org/content/aip/journal/jcp/59/12/10.1063/1.1680022http://aip.scitation.org/doi/10.1063/1.1680022.

[25] J. Čížek, J. Chem. Phys. **45**, 4256 (1966), ISSN 0021-9606, URL http://link.aip.org/link/?JCP/45/4256/1&Agg=doihttp://aip.scitation.org/doi/10.1063/1.1727484.

[26] R. M. Parrish, L. A. Burns, D. G. A. Smith, A. C. Simmonett, A. E. DePrince, E. G. Hohenstein, U. Bozkaya, A. Y. Sokolov, R. Di Remigio, R. M. Richard, et al., J. Chem. Theory Comput. **13**, 3185 (2017), ISSN 1549-9618, URL http://pubs.acs.org/doi/abs/10.1021/acs.jctc.7b00174http://pubs.acs.org/doi/10.1021/acs.jctc.7b00174.

[27] Q. Sun, T. C. Berkelbach, N. S. Blunt, G. H. Booth, S. Guo, Z. Li, J. Liu, J. D. McClain, E. R. Sayfutyarova, S. Sharma, et al., Wiley Interdiscip. Rev. Comput. Mol. Sci. **8**, e1340 (2018), ISSN 17590876, 1701.08223, URL http://doi.wiley.com/10.1002/wcms.1340.

[28] J. Kobus, Chem. Phys. Lett. **202**, 7 (1993), ISSN 00092614, URL http://linkinghub.elsevier.com/retrieve/pii/000926149385342L.

[29] F. Jensen, Theor. Chem. Acc. **113**, 187 (2005), ISSN 1432-881X, URL http://www.springerlink.com/index/10.1007/s00214-004-0618-8.

[30] T. G. Williams, N. J. DeYonker, and A. K. Wilson, J. Chem. Phys. **128**, 044101 (2008), ISSN 0021-9606, URL http://aip.scitation.org/doi/10.1063/1.2822907.

[31] A. D. Becke, J. Chem. Phys. **76**, 6037 (1982), ISSN 0021-9606, URL http://aip.scitation.org/doi/10.1063/1.445285http://aip.scitation.org/doi/10.1063/1.442958.

[32] S. Lehtola, M. Dimitrova, and D. Sundholm, arXiv p. 1812.06274 (2018), 1812.06274, URL http://arxiv.org/abs/1812.06274.

[33] N. S. Ostlund, J. Chem. Phys. **57**, 2994 (1972), ISSN 00219606, URL http://link.aip.org/link/?JCP/57/2994/1&Agg=doi.

[34] W. D. Edwards, Int. J. Quantum Chem. **34**, 549 (1988), ISSN 0020-7608, URL http://doi.wiley.com/10.1002/qua.560340859.

[35] S. Lehtola and H. Jónsson, J. Chem. Theory Comput. **10**, 5324 (2014), ISSN 1549-9618, URL http://pubs.acs.org/doi/abs/10.1021/ct500637x.

[36] D. W. Small, E. J. Sundstrom, and M. Head-Gordon, J. Chem. Phys. **024104** (2015), ISSN 0021-9606.

[37] S. Lehtola, M. Head-Gordon, and H. Jónsson, J. Chem. Theory Comput. **12**, 3195 (2016), ISSN 1549-9618, URL http://pubs.acs.org/doi/abs/10.1021/acs.jctc.6b00347.

[38] S. Lehtola, E. Ö. Jónsson, and H. Jónsson, J. Chem. Theory Comput. **12**, 4296 (2016), ISSN 1549-9618, URL http://pubs.acs.org/doi/abs/10.1021/acs.jctc.6b00622.

[39] E. A. McCullough, Comput. Phys. Reports **4**, 265 (1986), ISSN 01677977, URL http://linkinghub.elsevier.com/retrieve/pii/0167797786900201.

[40] J. Lehtola, M. Hakala, J. Vaara, and K. Hämäläinen, Phys. Chem. Chem. Phys. **13**, 5630 (2011), ISSN 1463-9084, URL http://pubs.rsc.org/en/content/articlehtml/2011/cp/c0cp02269ahttp://www.ncbi.nlm.nih.gov/pubmed/21283842.

[41] J. Rasch and A. C. H. Yu, SIAM J. Sci. Comput. **25**, 1416 (2004), ISSN 1064-8275, URL http://epubs.siam.org/doi/10.1137/S1064827503422932.

[42] D. Pinchon and P. E. Hoggan, Int. J. Quantum Chem. **107**, 2186 (2007), ISSN 00207608, URL http://doi.wiley.com/10.1002/qua.21337.

[43] B. Zhang, J. Yuan, and Z. Zhao, Comput. Phys. Commun. **194**, 84 (2015), ISSN 00104655, URL http://dx.doi.org/10.1016/j.cpc.2015.04.008http://linkinghub.elsevier.com/retrieve/pii/S0010465515001393.

[44] A. Gil and J. Segura, Comput. Phys. Commun. **108**, 267 (1998), ISSN 00104655, URL http://linkinghub.elsevier.com/retrieve/pii/S0010465597001264.

[45] B. I. Schneider, J. Segura, A. Gil, X. Guan, and K. Bartschat, Comput. Phys. Commun. **181**, 2091 (2010), ISSN 00104655, URL http://dx.doi.org/10.1016/j.cpc.2010.08.038http://linkinghub.elsevier.com/retrieve/pii/S0010465510003450.

[46] B. I. Schneider, J. Segura, A. Gil, X. Guan, and K. Bartschat, Comput. Phys. Commun. **225**, 192 (2018), ISSN 00104655, URL https://doi.org/10.1016/j.cpc.2017.12.013http://linkinghub.elsevier.com/retrieve/pii/S0010465517304186.

[47] T. Yanai, D. P. Tew, and N. C. Handy, Chem. Phys. Lett. **393**, 51 (2004), ISSN 00092614, URL http://linkinghub.elsevier.com/retrieve/pii/S0009261404008620.

[48] R. Peverati and D. G. Truhlar, J. Phys. Chem. Lett. **2**, 2810 (2011), ISSN 1948-7185, URL http://pubs.acs.org/doi/abs/10.1021/jz201170d.

[49] R. Peverati and D. G. Truhlar, Phys. Chem. Chem. Phys. **14**, 16187 (2012), ISSN 1463-9084, URL http://www.ncbi.nlm.nih.gov/pubmed/23132141.

[50] J.-D. Chai and M. Head-Gordon, J. Chem. Phys. **128**, 084106 (2008), ISSN 0021-9606, URL http://www.ncbi.nlm.nih.gov/pubmed/18315032.

[51] N. Mardirossian and M. Head-Gordon, Phys. Chem. Chem. Phys. **16**, 9904 (2014), ISSN 1463-9084.

[52] N. Mardirossian and M. Head-Gordon, J. Chem. Phys. **144**, 214110 (2016), ISSN 0021-9606, URL http://scitation.aip.org/content/aip/journal/jcp/144/21/10.1063/1.4952647.

[53] T. Leininger, H. Stoll, H.-J. Werner, and A. Savin, Chem. Phys. Lett. **275**, 151 (1997), ISSN 00092614, URL http://linkinghub.elsevier.com/retrieve/pii/S0009261497007586.

[54] Z. Romanowski, Mol. Phys. **107**, 1339 (2009), ISSN 0026-8976, URL http://www.tandfonline.com/doi/abs/10.1080/00268970902873554.

[55] J. R. Flores, E. Clementi, and V. Sonnad, J. Chem. Phys. **91**, 7030 (1989), ISSN 0021-9606, URL http://aip.scitation.org/doi/10.1063/1.457320.

[56] J. Flores, E. Clementi, and V. Sonnad, Chem. Phys. Lett. **163**, 198 (1989), ISSN 00092614, URL http://linkinghub.elsevier.com/retrieve/pii/000926148980034X.

[57] P. Manninen and J. Vaara, J. Comput. Chem. **27**, 434 (2006), ISSN 0192-8651, URL http://www.ncbi.nlm.nih.gov/pubmed/16419020.

[58] S. Lehtola, J. Comput. Chem. **36**, 335 (2015), ISSN 01928651, URL http://doi.wiley.com/10.1002/jcc.23802.

[59] T. Helgaker, P. Jørgensen, and J. Olsen, *Molecular electronic-structure theory* (John Wiley & Sons, Ltd., 2000), ISBN 0 471 96755 6.

[60] S. Lehtola, J. Chem. Theory Comput. p. acs.jctc.8b01089 (2019), ISSN 1549-9618, 1810.11659, URL http://arxiv.org/abs/1810.11659http://pubs.acs.org/doi/10.1021/acs.jctc.8b01089.

[61] J. Lehtola, P. Manninen, M. Hakala, and K. Hämäläinen, J. Chem. Phys. **137**, 104105 (2012), ISSN 1089-7690, URL http://www.ncbi.nlm.nih.gov/pubmed/22979848.

[62] S. Lehtola, P. Manninen, M. Hakala, and K. Hämäläinen, J. Chem. Phys. **138**, 044109 (2013), ISSN 1089-7690, URL http://www.ncbi.nlm.nih.gov/pubmed/23387570.

[63] C. Sanderson and R. Curtin, J. Open Source Softw. **1**, 26 (2016), ISSN 2475-9066, /dx.doi.org/10.21105/joss.00026, URL http://joss.theoj.org/papers/10.21105/joss.00026.

[64] C. Sanderson and R. Curtin, in *ICMS 2018 Math. Softw. – ICMS 2018*, edited by J. Davenport, M. Kauers, G. Labahn, and J. Urban (Springer, Cham, 2018), pp. 422–430, ISBN 978-3-319-96418-8, URL http://link.springer.com/10.1007/978-3-319-96418-8_50.

[65] T. Tsuchimochi and G. E. Scuseria, J. Chem. Phys. **133**, 141102 (2010), ISSN 1089-7690, URL http://www.ncbi.nlm.nih.gov/pubmed/20949979.

[66] T. Tsuchimochi and G. E. Scuseria, J. Chem. Phys. **134**, 064101 (2011), ISSN 1089-7690, URL http://www.ncbi.nlm.nih.gov/pubmed/21322655.

[67] F. Jensen, J. Chem. Phys. **115**, 9113 (2001), ISSN 0021-9606, URL http://link.aip.org/link/?JCP/115/9113/1http://link.aip.org/link/JCPSA6/v115/i20/p9113/s1&Agg=doihttp://aip.scitation.org/doi/10.1063/1.1413524.

[68] F. Jensen, J. Chem. Phys. **117**, 9234 (2002), ISSN 0021-9606, URL http://link.aip.org/link/?JCP/117/9234/1http://link.aip.org/link/JCPSA6/v117/i20/p9234/s1&Agg=doihttp://aip.scitation.org/doi/10.1063/1.1515484.

[69] F. Jensen and T. Helgaker, J. Chem. Phys. **121**, 3463 (2004), ISSN 0021-9606, URL http://link.aip.org/link/?JCP/121/3463/1http://aip.scitation.org/doi/10.1063/1.1756866.

[70] F. Jensen, J. Chem. Phys. **138**, 014107 (2013), ISSN 1089-7690, URL http://www.ncbi.nlm.nih.gov/pubmed/23298028.

[71] T. H. Dunning, J. Chem. Phys. **90**, 1007 (1989), ISSN 00219606, URL http://link.aip.org/link/JCPSA6/v90/i2/p1007/s1&Agg=doihttp://link.aip.org/link/?JCP/90/1007/1.

[72] R. A. Kendall, T. H. Dunning, and R. J. Harrison, J. Chem. Phys. **96**, 6796 (1992), ISSN 00219606, URL http://link.aip.org/link/JCPSA6/v96/i9/p6796/s1&Agg=doihttp://link.aip.org/link/?JCP/96/6796/1.

[73] N. B. Balabanov and K. A. Peterson, J. Chem. Phys. **123**, 64107 (2005), ISSN 0021-9606, URL http://www.ncbi.nlm.nih.gov/pubmed/16122300.

[74] J. Kobus, Phys. Rev. A **91**, 022501 (2015), ISSN 1050-2947, URL https://link.aps.org/doi/10.1103/PhysRevA.91.022501.

[75] J. Kobus, *Private communication*.

[76] F. Bloch, Zeitschrift für Phys. **57**, 545 (1929), ISSN 1434-6001, URL http://link.springer.com/10.1007/BF01340281.

[77] P. A. M. Dirac, Math. Proc. Cambridge Philos. Soc. **26**, 376 (1930), ISSN 0305-0041, URL http://www.journals.cambridge.org/abstract_S0305004100016108.

[78] J. P. Perdew and Y. Wang, Phys. Rev. B **45**, 13244 (1992), ISSN 0163-1829, URL http://link.aps.org/doi/10.1103/PhysRevB.45.13244.

[79] J. P. Perdew, K. Burke, and M. Ernzerhof, Phys. Rev. Lett. **77**, 3865 (1996), ISSN 0031-9007, URL http://www.ncbi.nlm.nih.gov/pubmed/22502509http://link.aps.org/doi/10.1103/PhysRevLett.77.3865.

[80] J. P. Perdew, K. Burke, and M. Ernzerhof, Phys. Rev. Lett. **78**, 1396 (1997), ISSN 0031-9007, URL http://link.aps.org/doi/10.1103/PhysRevLett.78.1396.

[81] C. Adamo and V. Barone, J. Chem. Phys. **110**, 6158 (1999), ISSN 0021-9606, URL http://link.aip.org/link/JCPSA6/v110/i13/p6158/s1&Agg=doihttp://aip.scitation.org/doi/10.1063/1.478522.

[82] M. Ernzerhof and G. E. Scuseria, J. Chem. Phys. **110**, 5029 (1999), ISSN 0021-9606, URL http://link.aip.org/link/JCPSA6/v110/i11/p5029/s1&Agg=doihttp://aip.scitation.org/doi/10.1063/1.478401.

[83] A. D. Becke, Phys. Rev. A **38**, 3098 (1988), ISSN 0556-2791, URL http://link.aps.org/doi/10.1103/PhysRevA.38.3098.

[84] J. Perdew, Phys. Rev. B **33**, 8822 (1986), ISSN 0163-1829, URL http://link.aps.org/doi/10.1103/PhysRevB.33.8822.

[85] C. Lee, W. Yang, and R. G. Parr, Phys. Rev. B **37**, 785 (1988), ISSN 0163-1829, URL http://link.aps.org/doi/10.1103/PhysRevB.37.785.

[86] A. D. Becke, J. Chem. Phys. **98**, 5648 (1993), ISSN 0021-9606, URL http://link.aip.org/link/?JCP/98/5648/1http://link.aip.org/link/JCPSA6/v98/i7/p5648/s1&Agg=doihttp://aip.scitation.org/doi/10.1063/1.464913.

[87] P. J. Stephens, F. J. Devlin, C. F. Chabalowski, and M. J. Frisch, J. Phys. Chem. **98**, 11623 (1994), ISSN 0022-3654, URL http://pubs.acs.org/doi/abs/10.1021/j100096a001.

[88] J. P. Perdew, A. Ruzsinszky, G. I. Csonka, L. A. Constantin, and J. Sun, Phys. Rev. Lett. **103**, 026403 (2009), ISSN 0031-9007, URL http://link.aps.org/doi/10.1103/PhysRevLett.103.026403.

[89] J. P. Perdew, A. Ruzsinszky, G. I. Csonka, L. A. Constantin, and J. Sun, Phys. Rev. Lett. **106**, 179902 (2011), ISSN 0031-9007, URL http://link.aps.org/doi/10.1103/PhysRevLett.106.179902.

[90] G. I. Csonka, J. P. Perdew, and A. Ruzsinszky, J. Chem. Theory Comput. **6**, 3688 (2010), ISSN 1549-9618, URL http://pubs.acs.org/doi/abs/10.1021/ct100488v.

[91] J. Sun, R. Haunschild, B. Xiao, I. W. Bulik, G. E. Scuseria, and J. P. Perdew, J. Chem. Phys. **138**, 044113 (2013), ISSN 0021-9606, URL http://aip.scitation.org/doi/10.1063/1.4789414.

[92] S. Boys and F. Bernardi, Mol. Phys. **19**, 553 (1970), ISSN 0026-8976, URL http://www.tandfonline.com/doi/abs/10.1080/00268977000101561.

[93] F. Jensen, J. Chem. Theory Comput. **10**, 1074 (2014), ISSN 1549-9618, URL http://pubs.acs.org/doi/abs/10.1021/ct401026a.